# Simulation and experimental analysis of optical frequency comb generation methods and its application in high-capacity optical communication systems

*Narmada Rajaram*

Thesis submitted to the University of Ottawa in partial Fulfillment of the requirements for the Masters in Applied Science degree

in

Electrical and Computer Engineering


School of Electrical Engineering and Computer Science

Faculty of Engineering

University of Ottawa

# ABSTRACT

The exponential growth of data usage is reshaping optical communications networks and driving us to look for innovative technologies. Increased bandwidth, faster speeds, scalability are the needs for today's telecommunication field. These needs can be met, and the transmission ability can be increased by adopting advanced modulation formats, increased data rate and increasing the number of optical carriers. Increasing the number of optical carriers seem to be a captivating technology as the well-established dense wavelength division multiplexing (DWDM) is being used to multiplex several optical carriers in an optical communication system. High-capacity optical communication systems can be implemented using DWDM technique, which allows the transmission of separate wavelengths over a single optical channel. One of the challenges of DWDM is precise wavelength control to avoid crosstalk. Also, the use of discrete single wavelength lasers consumes lot of energy and make the system expensive. Replacing multiple laser sources with a single laser with multiple carriers in a DWDM system is a novel technique leading to reduced energy consumption, system complexity and cost. Optical frequency comb (OFC) is a multi carrier single laser source which can be integrated with the DWDM system. OFC is a promising technology which find its application in communication system as they offer many advantages such as high repetition rates, low noise, high stability covering multiple communication bands. This makes them ideal for advanced communication system.

In this thesis we shall see the OFC generation using passive mode locked Quantum Dash laser and electro-optic modulation technique. Experimental results and analysis for varying temperatures for Quantum Dash laser are presented and their effect is studied. The fundamental mode locking characteristics are studied and experiments are carried out to find the repetition rate and results of RF spectra measurement are presented. Experimental results to measure the dispersion of the laser cavity are also presented. OFC generation with good flatness is obtained using electro-optic modulator called the fibre loop modulation technique. Experimental results for OFC generation are presented and compared with the simulation results. Simulation is performed using the commercially available simulation software – OptiSystem. Comb line characteristics of OFC is analysed with respect to the amplitude of the RF signal used in fibre loop modulation technique. A direct relation between the amplitude of RF signal and the number of comb lines is obtained and the simulation results of the same is presented in this work.

A system is modelled integrating OFC in DWDM communication system in which the transmission medium considered is free-space. Simulation results are presented showing the potential of OFC to support high-capacity optical communication. Performance analysis of the system in terms of bit error rate and range of the optical transmission is presented which show that the modelled system is capable of high-capacity communication system.

# ACKNOWLEDGMENTS

First and foremost, I would like to express my profound gratefulness to my supervisor Prof (Dr) Trevor James Hall. His guidance, support and encouragement have been instrumental throughout the course of my thesis. This work would not have been possible without his invaluable help and unwavering understanding. Prof Hall has been a guiding force, not just in my academic journey but also in personal growth. His ability to balance empathy and professionalism has left a lasting impression in me. I am constantly inspired by his immense knowledge and polymathic abilities, which extend far beyond his field of expertise. I have cherished every discussion with him—whether about the intricacies of my research, broader academic concepts, or even topics beyond the realm of studies. These conversations have been deeply enriching and have shaped my thinking in countless ways. I feel incredibly fortunate to have been one of his students and will always carry the lessons I've learned from him into my future endeavors. I remain deeply indebted and eternally grateful for all he has done.

I would also like to extend my heartfelt thanks to Prof Karin Hinzer. Her encouragement and the opportunities she provided have been immensely helpful in my learning and development. Without these opportunities, my thesis would not have been possible, and her support motivated me throughout this journey. Additionally, I am deeply grateful to Ahmad Atieh whose dedication to mentorship has had a profound impact on my academic progress. His willingness to help whenever I needed it and his incredible ability to transfer knowledge has been invaluable.

The experimental work that I carried out at the National Research Council, Canada played a significant role in my thesis, and I would like to express my gratitude to Zhenguo Lu, Jiaren Liu, Philip J. Poole for their support. Special thanks to Chun-Ying Song who is an outstanding teacher and whose expertise made my laboratory learning experience an exceptional one. I am deeply appreciative of all that she taught me. I thank my lab mate Jaskiran Kaur for a fun and great work together at the lab. Many thanks to the members of SUNLAB especially John Cook, Paige Wilson, Christine Couture for their constant support. Additionally, I would also like to thank our collaborators Prof Liam Barry and Mahrokh Avazpour from Dublin City University, Ireland for their support and sharing experimental results.

I would like to extend my deepest gratitude to my friends and family who have supported me throughout. Notable thanks to my friend Abhilash for introducing me to the wonders of Physics

and igniting a passion for the subject and also teaching valuable life lessons. Words fall short in expressing my gratitude to my parents Vasanthi and Rajaram whose endless love, sacrifices and unwavering support have been the greatest source of strength in my life. Special mention to my brother Vasanth for being a source of joy and enjoyment. Lastly, special note of gratitude goes to my beloved friend Shyam Kishore Pandian for taking such good care of me and making my life so much easier and fulfilling in Canada. Your support means the world to me and thanks for being a constant in my life. I am truly blessed to have you in my life.

## Contents

# List of Publications

1. **N. Rajaram**, M. Avazpour, L. Barry, K. Hinzer, T. Hall and A. Atieh, "System Modelling, Numerical Simulations and Experimental Validation of High Capacity FSO Data Transmission in DWDM Communication Employing Optical Frequency Comb," 2024 International Conference on Numerical Simulation of Optoelectronic Devices (NUSOD), New Delhi, India, 2024, pp. 1-2, https://doi.org/10.1109/NUSOD62083.2024.10723468

2. M. Avazpour, **N. Rajaram**, A. Atieh, and L. Barry, "Optical Frequency Comb Generation for DWDM Free Space Optical Communication Links," in Advanced Photonics Congress 2024, Technical Digest Series (Optica Publishing Group, 2024), paper NeTh1C.4. https://dx.doi.org/10.1364/NETWORKS.2024.NeTh1C.4

3. I. A. Ali, D. P. Wilson, M. N. Beattie, R. Hogan, **N. Rajaram**, R. Cheriton, A. Atieh, and K. Hinzer, "A Free Space Optical Link Model for C-band Data and Power Transmission," in Advanced Photonics Congress 2024, Technical Digest Series (Optica Publishing Group, 2024), paper JTu1A.18. https://dx.doi.org/10.1364/BGPP.2024.JTu1A.18

4. Idriss Amadou Ali, D. Paige Wilson, Meghan N. Beattie, Ryan Hogan, **Narmada Rajaram**, Ross Cheriton, Ahmad Atieh, Karin Hinzer, "A free space optical link model for C-band data and power transmission," Proc. SPIE 12877, Free-Space Laser Communications XXXVI, 128771Q (12 March 2024); https://doi.org/10.1117/12.3001939

# List of Figures

# Chapter 1 Introduction

## 1.1. Background and motivation

The telecommunications industry has witnessed rapid evolution over the past few decades, driven by the insatiable demand for higher data rates and greater connectivity. The advancements of technologies such as 5G, Internet of Things (IoT), and cloud computing has further accelerated the need for innovative solutions. Fiber-optic networks, characterized by their high capacity and low signal attenuation, have become the backbone of global telecommunications infrastructure. Among the key technologies enabling this transformation is Dense Wavelength Division Multiplexing (DWDM), which allows transmission of multiple optical signals at different wavelengths within the same optical fiber, thereby increasing the capacity of the system.

However, as the demand for bandwidth grows, conventional DWDM systems face challenges such as limited spectral efficiency, nonlinear impairments, and energy consumption. To address these issues, there is a pressing need for advanced light sources that can generate stable, densely packed, and precisely spaced wavelength channels. Optical Frequency Combs (OFCs) have emerged as a groundbreaking technology offering a transformative approach to optical communication by generating multiple wavelength channels for high-capacity data transmission.

Introduced through the pioneering work in mode-locked lasers, OFCs consist of a series of discrete, equally spaced optical frequencies resembling the teeth of a comb. This revolutionary concept was first applied in metrology and spectroscopy, leading to Nobel Prize-winning advancements in optical frequency measurements. The motivation behind studying OFCs lies in their ability to bridge the gap between microwave and optical frequencies, enabling high precision and coherence. In telecommunications, OFCs offer a highly scalable and efficient solution to meet the growing demands of high-capacity data transmission. Their ability to generate densely packed wavelength channels makes them an ideal candidate for Dense Wavelength Division Multiplexing (DWDM) systems which is crucial for modern optical networks. Furthermore, OFCs support advanced modulation schemes and coherent detection techniques thus increasing spectral efficiency and minimizing errors. The inherent characteristics of OFCs also addresses critical

challenges in optical communication systems. For instance, their ultra-wideband nature and precise frequency spacing enable seamless integration into photonic networks.

This thesis aims to explore the simulation and experimental analysis of optical frequency comb generation and its applications in high-capacity optical communication systems. By leveraging the unique properties of OFCs, this work seeks to contribute to the development of next-generation communication technologies.

## 1.2. Thesis Outline

This thesis is structured into six chapters which aims to describe the concepts of optical frequency combs, its generation methods and application in DWDM communication systems.

Chapter 1 describes the background and motivation to carry out the research by exploring the advancements in modern telecommunication systems and the challenges faced. It introduces the concept of OFCs as an innovative technology and outlines their significance in DWDM systems. The chapter also highlights the motivation behind the study emphasizing the need for efficient high-bandwidth optical communication solutions.

Chapter 2 provides an introduction to OFCs and their characteristics. It gives a general overview of OFCs followed by discussion on their characteristics. Two methods of OFC generation namely using mode-locked laser and electro-optic modulation is briefly discussed here. This chapter also examines the various parameters associated with OFCs namely fundamental repetition rate, spectral bandwidth, flatness of OFC and timing jitter. This chapter provide an insight for the application of OFC in DWDM system.

Chapter 3 discusses in detail about OFC generation using passive mode-locked Quantum Dash laser. The concept of density of states and how carrier confinement leads to improved lasing efficiency is discussed. A comprehensive description of experimental setup, procedures and results on mode locking characteristics of QDash laser is presented. Experiments conducted under varying conditions are analyzed to identify the factors influencing the OFC. Additionally, this chapter talks about dispersion and an expression to determine it is derived. Experiments are conducted to measure dispersion at different temperatures and the results are presented. This chapter is presented in the context of a novel and emerging method of OFC generation for its application in modern telecommunication systems.

Chapter 4 focuses on the generation of OFC using fibre loop modulation technique – an electro-optic modulation based method. It begins by detailing the underlying principle of comb generation and the mathematical expression for OFC generation using this method is derived. Numerical simulations have been performed and the result of the generated OFC is presented. Simulations were also performed with varying conditions to analyze the comb characteristics and results are presented. Experiments were conducted to generate OFCs using the fibre loop modulation technique and their results are validated by simulations. It has been found that a good agreement is obtained between the experimental and simulation results. This study provides an insight to the properties of generated combs and how they can be modified to suit our application.

Chapter 5 introduces Dense Wavelength Division Multiplexing (DWDM) technology and its integration with Free Space Optical (FSO) communication systems. The discussion begins with overview of DWDM and FSO communication and its relevance in modern telecommunication networks. A key focus is placed on analyzing the wavelength dependence on the atmospheric attenuation in FSO systems. The chapter further presents a proposed model of a communication system that integrates OFCs in DWDM system for data transmission over FSO channel. Numerical simulations are performed to evaluate the performance of the system demonstrating its capability to transmit high-capacity data over long transmission range. Detailed analysis based on the results highlights the advantages and potential applications of the proposed approach in next generation communication systems.

Chapter 6 provides a comprehensive summary of the work conducted in this thesis, highlighting the key findings and contributions.

This research work advances the understanding of OFC generation methods and explores their practical application in DWDM communication system, offering valuable insights for future technologies.

# Chapter 2 Optical frequency comb

## 2.1. Introduction to Optical frequency comb

Optical frequency comb is a comb of frequencies which are equivalently distributed with a broad optical spectrum in the frequency domain. These frequencies are given by the expression:

$$f_n = nf_r + f_o \tag{2.1}$$

where $f_r$ is the repetition rate of the comb which is the frequency difference between two adjacent comb lines, whereas $f_o$ is an offset frequency. Figure 2.1 shows the representation of OFC in frequency and time domain. Each line in the frequency domain represents distinct optical frequency. In the time domain this is a train of optical pulses. The spacing of the combs in frequency domain i.e. $f_r$ is related to the time domain such that it is inversely proportional between the pulses. The bandwidth of the optical spectrum denoted by $\Delta\nu$ is related to the shortness of the pulse in time domain as shown in Figure 2.1.

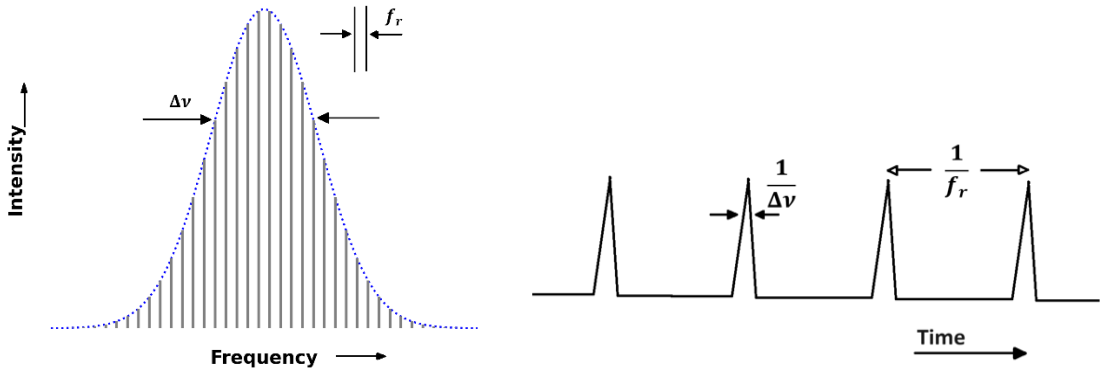


(a) (b)

Figure 2.1 (a) Frequency domain and (b) time domain representation of OFC

## 2.2. Methods of OFC generation

OFC can be generated using various techniques such as electro-optic modulation, mode locked lasers, using resonators etc. In this work we shall see the OFC generation based on electro-optic

modulation and mode locked laser. Before going in detail of the comb generation, let us see the concepts of electro-optic modulation and mode locked laser.

### 2.2.1. Electro-optic modulation

OFC generation using electro-optic effect are called electro-optic combs (EOC). The electro-optic effect is a phenomenon that modifies the refractive index of a material by applying electric field. Electro- optic phenomena include several effects such as Pockels effect and Kerr effect. Pockels effect is most widely used in the existing electro-optic modulators (EOM). It is a phenomenon where the refractive index changes linearly in response to applied electric field. As the refractive index changes with the electric field, the optical phase of light travelling through the material is modulated. The most widely used EOM is the Mach-Zehnder interferometer which overcomes the drawbacks of the basic architecture of EOM such as requirement of applied electric field reaching in kilovolts, easily subjected to parasite effects. Figure 2.2 shows the design of a dual-drive Mach-Zehnder modulator (MZM).

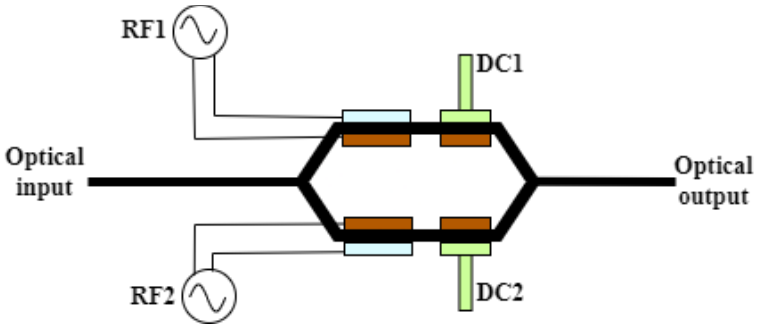


Figure 2.2 Dual-drive Mach-Zehnder modulator

The Mach-Zehnder structure consists of an input optical branch which splits the incoming optical signal into two arms. Both the arm of the modulator is covered with electrodes that is used to apply RF signal and static voltage. Both voltages induce electro-optic effect and at the output both the arms are recombined leading to an interference effect. The static voltage sets the modulator at a specific operating point where modulation is most efficient. When RF signal is applied, the refractive index changes linearly resulting in phase shift of the optical signal. This phase shift modulates the output optical signal.

### 2.2.2. Mode locked laser

The term mode locking refers to locking up the phases of the modes of the laser by some techniques. The mode locking phenomenon can be better understood in time domain and is represented below in Figure 2.3. In the figure, three modes are considered, and their phases interact constructively at some point giving rise to high intensity pulses. The interval between these pulses is given by the round-trip time $T_{RT}$. There are three types of mode locking techniques namely active, passive and hybrid by which the phases of the modes can be locked. Table 2.1 lists the main features of these three mode-locking techniques.

In active mode locking, an external signal is applied to modulator which periodically changes the loss in the cavity. A periodic modulation signal usually an RF signal is applied to the modulator. The modulator changes the loss in cavity by reducing the loss at specific time allowing the light to build up and form a pulse. When the loss is high the intensity of light decreases. This process is synchronized with the cavity round trip time so that the pulses are formed at regular intervals. Active mode locking provides the lowest timing jitter among the three mode locking techniques.

In case of passive mode locking, instead of using an external modulator a non-linear component called saturable absorber is placed inside the laser cavity. The most widely used saturable absorber is SESAM (Semiconductor Saturable Absorber Mirror). It consists of a layer of materials that absorbs light on top of a high reflectivity mirror. Materials like InGaAs or GaAs are commonly used to make saturable absorbers, and these materials are grown of reflective structure to create SESAM. The saturable absorber selectively absorbs light at low intensities and transmit light at high intensity. The pulse formed is circulated within the cavity by gaining energy from the gain medium creating a feedback loop. Under stable mode locking condition, only one pulse exists at a time in the cavity and each pulse is separated by the round-trip time. Passive mode locking produces short pulses with high intensity.

Hybrid mode locking combines the technique of both active and passive mode locking. In this case an external signal is applied either to the gain or saturable absorber section. The shaping and shortening of pulse are assisted by the saturable absorber. This method results in short and low jitter pulses taking the advantage of both active and passive mode locking techniques.

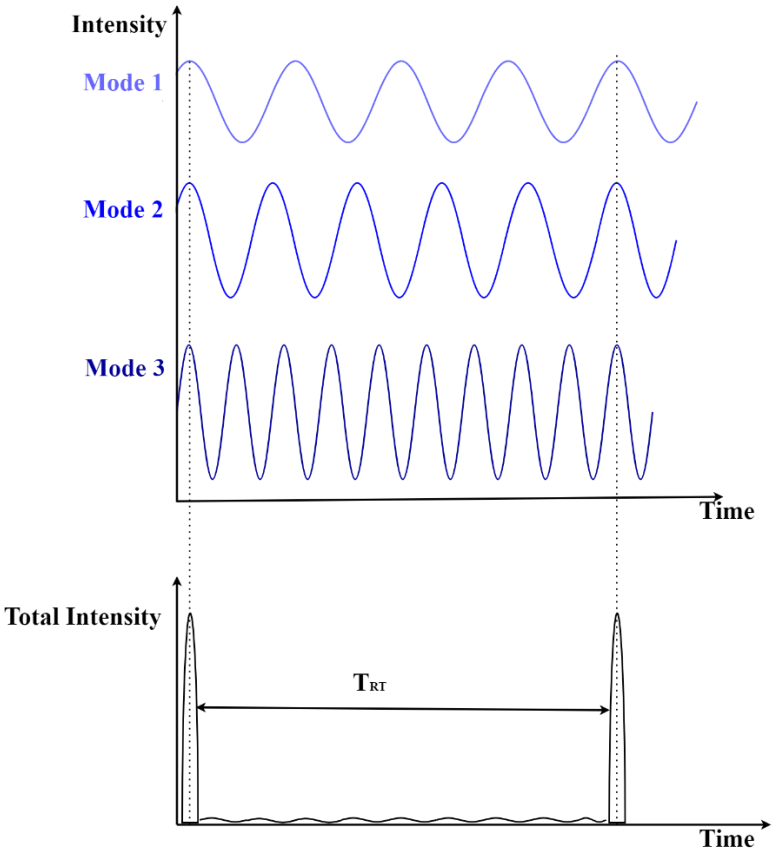


Figure 2.3 Phase locking in MLL

| **Features** | **Active MLL** | **Passive MLL** | **Hybrid MLL** |
|---|---|---|---|
| Repetition rate | Comparatively low (Tens of GHz) | High (THz) | Comparatively low (Tens of GHz) |
| Tunability of spectral bandwidth | Flexible | Rigid | Flexible |
| Timing jitter | Lowest | Highest | Relatively low |
| Tunability of repetition rate | Flexible | Rigid | Flexible |
| External signal | Required | Not required | Required |
| Design | Complex | Simple | Relatively complex |

Table 2.1 Comparison of mode locking techniques (Reference [27])

## 2.3. Parameters of OFC

In this section we shall see some of the important parameters of OFC. As our work focuses on the application of OFC in optical data transmission, some of the important terms related to this application will be discussed.

### 2.3.1. Fundamental repetition rate

The fundamental repetition rate is defined as the frequency at which pulses are generated. It corresponds to the inverse of the round-trip time $T_{RT}$ (time taken for light to complete exactly one round trip of the laser cavity L) and is given by,

$$f_{rep} = \frac{1}{T_{RT}} = \frac{c}{2nL} \tag{2.2}$$

where c is the speed of light in vacuum, n is the refractive index of the medium inside the cavity and L is the laser cavity length. In case of passive mode locked laser, the repetition rate can be designed and fixed by careful engineering of the laser cavity length. Generally, a high repetition rate is desirable for OFC based optical data transmission as they are less susceptible to interference between the adjacent combs and also making the filtering process simple.

### 2.3.2. Spectral bandwidth

The spectral bandwidth refers to the range of frequencies in the OFC. This width is generally defined as the 3dB bandwidth or full width at half maximum (FWHM) of the emission spectra. It is an important characteristic of OFC. The spectral width is given by,

$$\Delta\lambda_{BW} = \lambda_1 - \lambda_2 = \frac{c}{f_1} - \frac{c}{f_2} \tag{2.3}$$

where $\lambda_1$ and $\lambda_2$ are the upper and lower half power points respectively. The wavelength at the centre of the spectral bandwidth called the centre wavelength is also an important consideration as the existing components of telecommunication system can be integrated to the OFC source. The centre wavelength for a semiconductor laser is given by,

$$\lambda_c = \frac{hc}{E_g} \tag{2.4}$$

where $h$ is the Planck constant, $c$ is the speed of light at vacuum and $E_g$ is the energy gap of the semiconductor material. Hence with proper selection of material and device engineering the MLL can be designed for specific wavelengths. Considering the same repetition rate, for an OFC based data transmission large spectral bandwidth is desired as it has large number of comb lines.

### 2.3.3. Flatness of OFC

For a high-performance optical data transmission, the power of each comb line in the OFC is desired to be approximately same. This parameter is called the flatness of OFC. In practical frequency combs the power level of each comb decreases as we move away from optical spectrum bandwidth. Having an uniform power level ensures that each channel corresponding to the comb line has the same signal strength and thus improving the efficiency and balance of the data transmission system. A high output power is essential for optical data transmission as it will eliminate the need for optical amplifier which induces amplified spontaneous emission (ASE) noise in the system thus increasing the signal to noise ratio.

### 2.3.4. Timing jitter

Timing jitter is defined as the variation in the arrival of pulses from its original position in time domain. Timing jitter is related to the phase noise in the frequency domain. Timing jitter is critical in OFC as it affects the precision of the pulse intervals and the coherence of the comb lines. This may lead to degradation of signal integrity and increased bit error rate.

## 2.4. Summary

This chapter introduces Optical frequency comb and their representation in time and frequency domain. A brief overview of the methods of OFC generation namely electro-optic modulation technique and mode locked laser is provided. The principles of mode locking along with different types of mode locking is explained and a comparison between the different mode locking techniques is shown. Various features of OFC in the context for its application in optical data

transmission is presented. It is concluded that an OFC with high repetition rate, broad spectral bandwidth, uniform power level across all the individual combs (flatness), minimal timing jitter are desired for optimal performance in advanced communication systems.

# Chapter 3 OFC generation using Quantum Dash laser

## 3.1. Introduction

One of the breakthrough inventions of the twentieth century is the development of semiconductor lasers. These lasers find their applications in everyday life like laser printing, projectors; industrial applications like LiDAR; medical applications like LASIK surgery, imaging; in scientific research such as spectroscopy, quantum computing etc. The application of semiconductor laser in optoelectronics has become the core for telecommunication today due to their advantages such as small size, low input energy and long life.

The first semiconductor laser operation was demonstrated in 1962. This laser had p-n junction based on GaAs as the active medium with polished facets providing the optical feedback enabling lasing action through stimulated emission by injecting current. The drawback of this structure was poor carrier confinement and high optical losses. A significant improvement over this design was the introduction of double-heterostructure laser where a layer of one semiconductor material was sandwiched between two cladding layers of another semiconductor material which has relatively higher band gap energy. This causes the injection carriers to be trapped inside the active region leading to higher efficiency. Since then, various progress towards improved performance have been developed including carrier confinement. In the next section we shall see how carrier confinement can lead to improved lasing efficiency.

## 3.2. Density of States

Density of states (DoS) describes the number of allowed states that the carriers can occupy. It has been realised through various studies that by reducing the dimensionality of the active region, carrier confinement can be achieved which in turn improves the lasing efficiency. The dimensionality here refers to the directions in which the carriers can move. The three-dimension structure is the bulk semiconductor whereas reducing the dimensionality to 2D we get quantum well structure. This can be achieved by reducing the structure below the de Broglie wavelength. Quantum wires structures are those whose dimensionality is reduced to 1D. When the structure is reduced in size in all the three directions, maximum quantum confinement is achieved. Such structures are called Quantum Dots (QD). The number of energy states that the carriers can be

present is dependent on quantum confinement effects. Figure 3.1 shows the carrier confinement and their respective density of states for all the cases discussed above.

It is observed from Figure 3.1 that as the number of dimensions is reduced, the available DoS is limited. The DoS for quantum dot is a delta like function indicating that the carriers can occupy single state. This leads to rapid filling of state resulting in lower threshold current and thus high optical gain. Quantum dots laser produces narrow linewidths resulting in single wavelength or narrowband emission spectra. They are ideal for applications such as precision metrology, spectroscopy, atomic clocks etc.

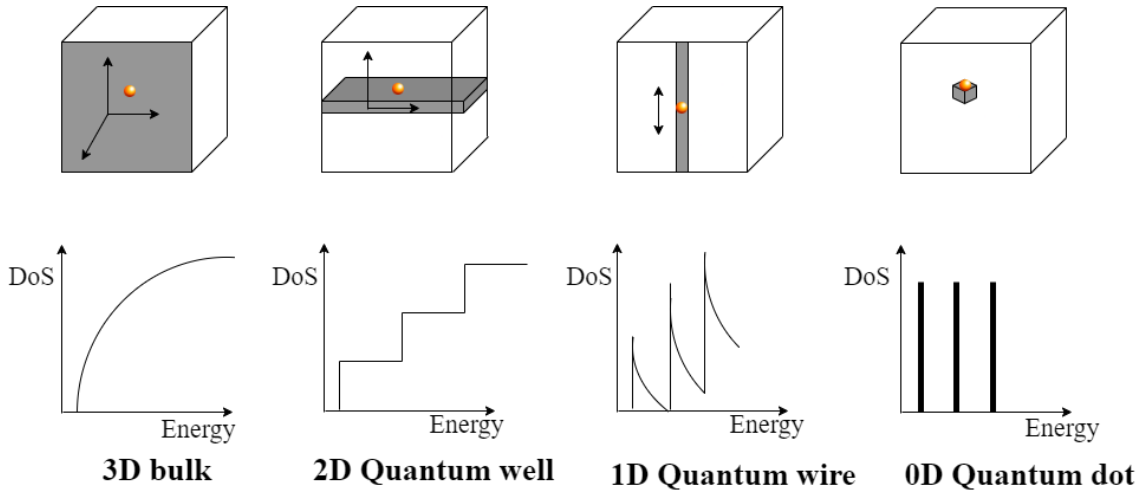


Figure 3.1 Density of states as a function of dimension of carrier movement

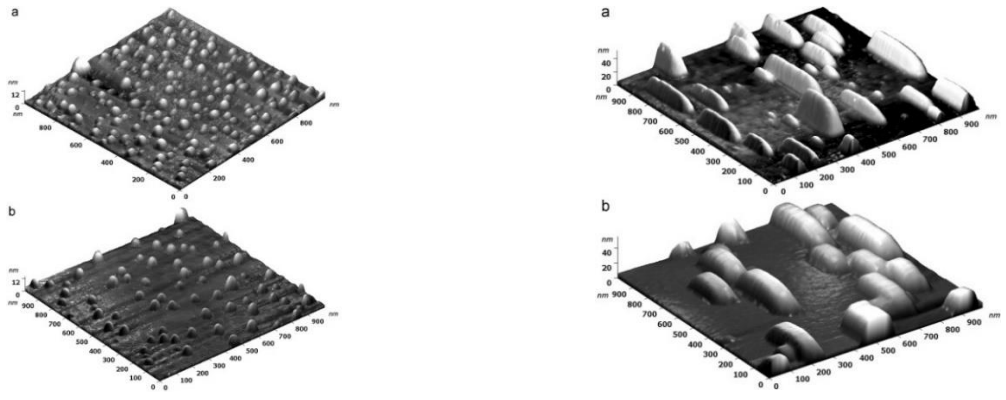


Figure 3.2 AFM images of QD and QDash structure with varying densities. Reproduced from [7]

Through various research it has been found that under certain conditions the QD become elongated in one direction. These elongated structures are called Quantum Dash (QDash). QDash structure allows some freedom of movement in the elongated direction creating a quasi-0D confinement. QDash are better than QD in aspects such as they have larger fill factor thus leading to better carrier capture. Hence, they exhibit higher gain than QD. The QDash laser have broader gain spectra which is advantageous in applications like broadband emission making them suitable for multi-wavelength applications. Figure 3.2 shows the atomic force microscopy (AFM) images of QD and QDash structure with varying densities.

## 3.3. Mode locked QDash laser

Passive mode locked QDash laser generates frequency combs having a broad spectrum. They offer many advantages such as low threshold current density, broad emission spectrum, ultrafast carrier dynamics, good temperature stability. Another important advantage of using mode locked QDash laser is their operation into the C-band near 1550nm because the optical losses are minimum in this range for long optical communications. The experiments conducted on QDash devices in this thesis was provided by collaborators at the National Research Council, Canada. Figure 3.3 shows the cross-sectional image and schematic diagram of QDash laser. The devices used for experiments in this work has a similar structure as shown in Figure 3.3. The detailed fabrication process and device growth is explained in [9].

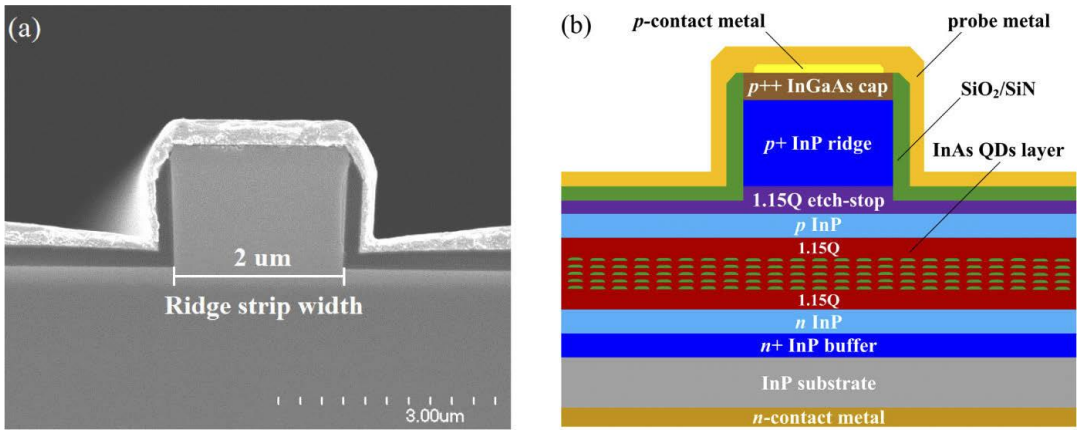


Figure 3.3 (a) Cross-sectional scanning electron microscopy image (b) Schematic cross-sectional diagram of passive mode locked QDash laser. Reproduced from [8]

## 3.4. Experiments on mode locking characteristics of comb QDash laser

Experiments were carried to study the performance of the QDash laser and the mode locking characteristics. The following tests were conducted-

i. L-I curve measurements
ii. Spectral measurements of optical combs
iii. RF spectra measurements of optical combs

The detailed experimental setup and the procedure are explained in the coming sections. All the experiments were carried out at National Research Council, Canada premises.

### 3.4.1. L-I curve measurements

The measurement of laser output power with respect to the bias current is the L-I measurement. This is the basic and first test to be carried out on the device as it used to check whether the device is working properly. Figure 3.4 shows the experimental setup for the test.

The QDash sample is mounted manually and two probes are contacted to inject current to the sample and ground. The thermoelectric controller (TEC) is used to inject current to the sample and set temperature. The sample is then enclosed in a chamber to maintain the humidity level. A LabView program is used to make fine adjustments to the alignment of the sample to capture the maximum output power and also to maintain and monitor the humidity level. The light output is collected by the photodiode which converts the optical signal to electrical signal which can then be read by the power meter. Careful consideration is given to the dew point of the environment and the working temperature when carrying out the experiments to avoid condensation on the sample. Figure 3.5 shows the actual experimental setup with chamber enclosure.

Temperature is set using the TEC controller and current is varied gradually while noting down the corresponding output power via the power meter. Experiments were conducted at four different temperatures from $20°C$ to $35°C$ in steps of $5°C$ . Figure 3.6 shows the plot between measured output power and the bias current for four different temperatures. It is observed from the plot that as the temperature increases the threshold current also increases. Table 3.1 shows the threshold current for different temperatures.

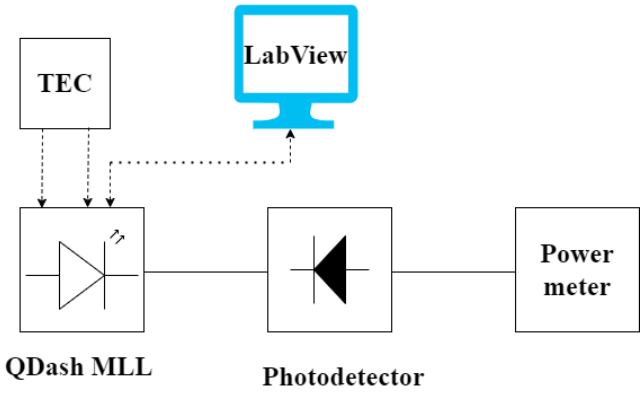


Figure 3.4 Experimental setup for L-I measurements

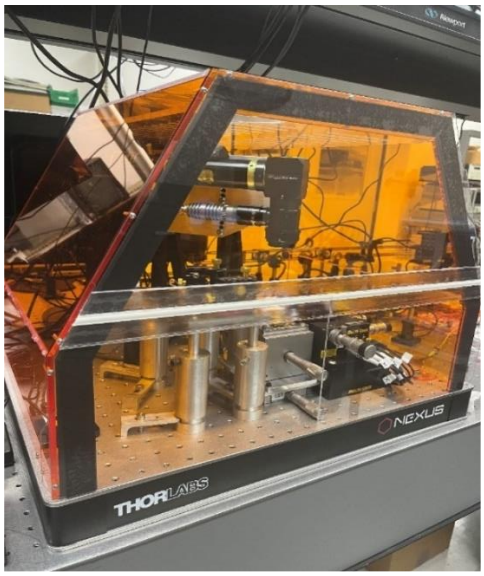


Figure 3.5 Actual experiment setup showing the chamber enclosure

| Temperature ($°C$) | Threshold current (mA) |
|---|---|
| 20 | 51 |
| 25 | 54 |
| 30 | 58 |
| 35 | 62 |

Table 3.1 Threshold current at various temperatures

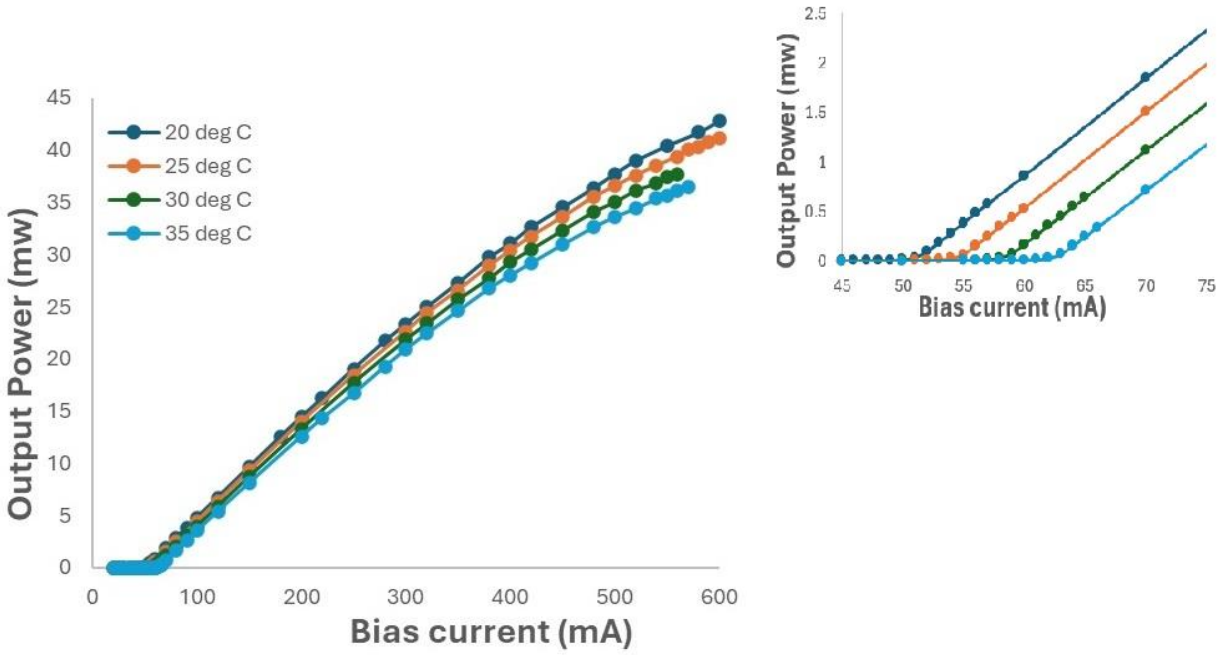


Figure 3.6 L-I characteristics of QDash sample at different temperatures

### 3.4.2. Spectral measurements of optical combs

This test was carried out to analyse the spectral characteristics of the sample. Figure 3.7 shows the experimental setup for the test. The temperature is set using the TEC controller and test was carried out at two temperatures viz. $22°C$ and $30°C$ . The light output is given to an isolator to transmit light in one direction and avoid any feedback. A 10/90 coupler is used to give 10% of output power to the power meter via the photodiode and 90% of output power is given to the optical spectrum analyzer (OSA) to measure the spectrum.

The bias current was varied from 150 mA and the corresponding emission spectra of the sample was measured using the optical spectrum analyzer. We measure the 3dB optical bandwidth also known as the FWHM and the centre wavelength. Figure 3.8 (a) and (b) shows the optical spectrum measured at $22\,°C$ and $30\,°C$ for different bias current and Table 3.2 shows the spectral measurements at these conditions. We conclude from the experimental results that as the bias current is increased the 3dB bandwidth also increases thus generating more number of combs. It is observed that with the increase in the bias current the centre wavelength shifts towards the longer wavelength of the spectrum. We also observe that at a constant bias current the spectrum shifts towards the longer wavelength with increase in temperature. This is illustrated in Figure 3.9, and

it shows the optical spectrum measured at 350mA for temperature 22°$C$ and 30°$C$. This test gives us an important estimate of the capability of the optical transmission of the device.

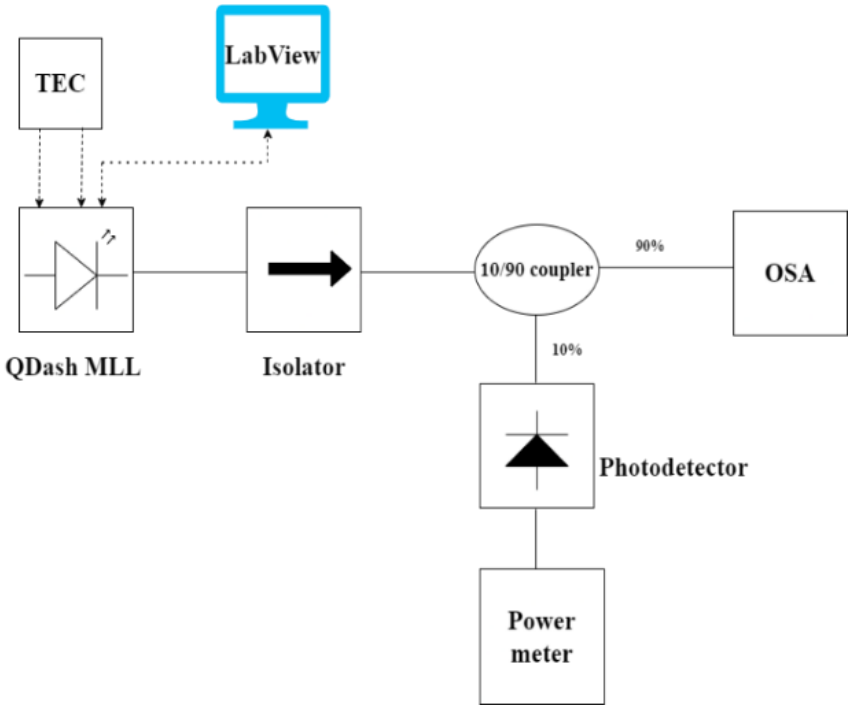


Figure 3.7 Experimental setup for spectral measurement

| Current (mA) | 3dB bandwidth (nm) | Centre wavelength (nm) |
|---|---|---|
| 250 | 9.08 | 1545.94 |
| 350 | 10.2 | 1548.42 |
| 450 | 12.08 | 1550.56 |

(a)

| Current (mA) | 3dB bandwidth (nm) | Centre wavelength (nm) |
|---|---|---|
| 150 | 7.04 | 1547.08 |
| 250 | 9.12 | 1549.84 |
| 350 | 10.08 | 1552.4 |
| 450 | 11.04 | 1555.04 |

(b)

Table 3.2 Spectral measurements for (a) 22°$C$ and (b) 30°$C$

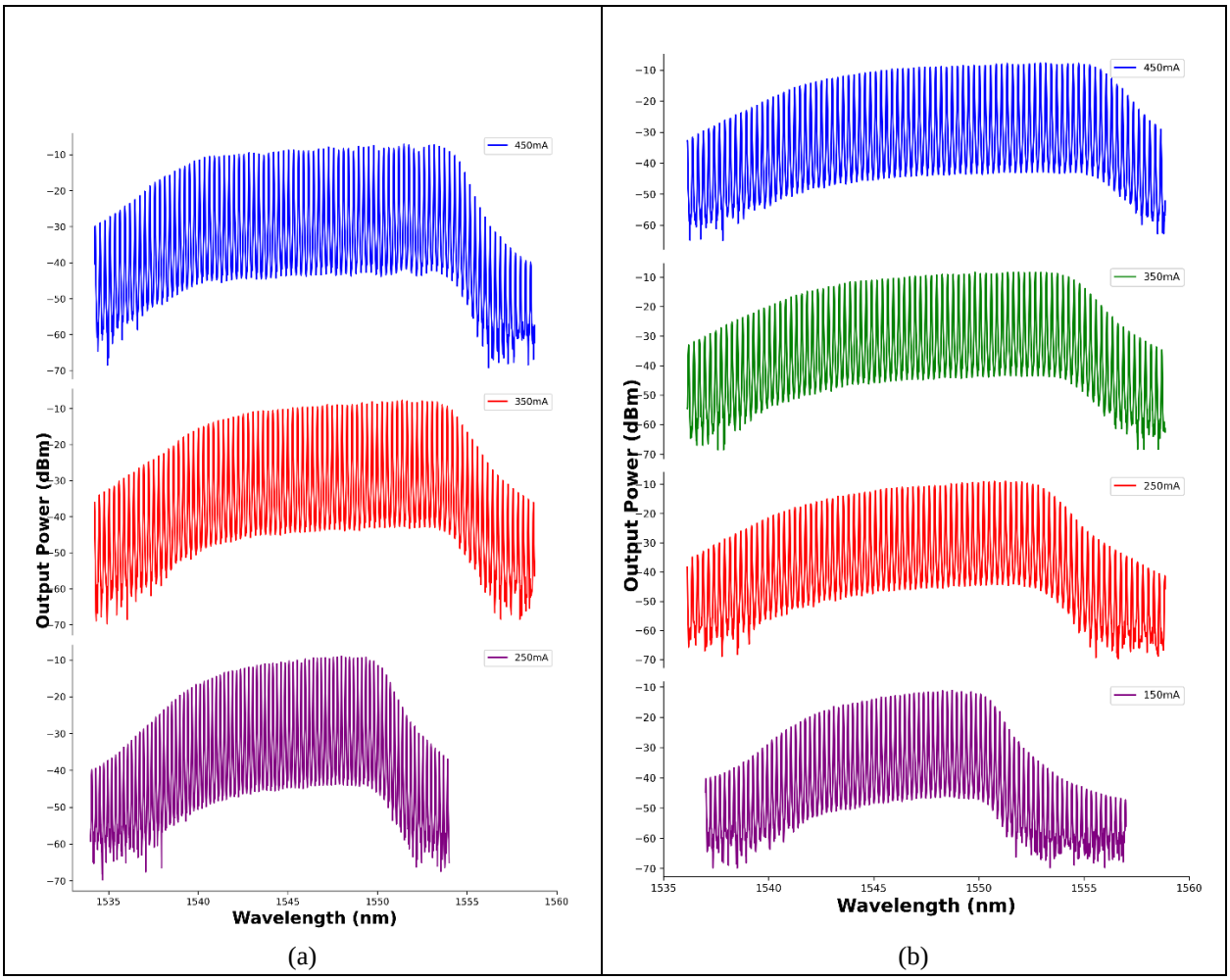


Figure 3.8 Optical spectrum measurement at different currents for (a) 22°$\boldsymbol{C}$ and (b) 30°$\boldsymbol{C}$

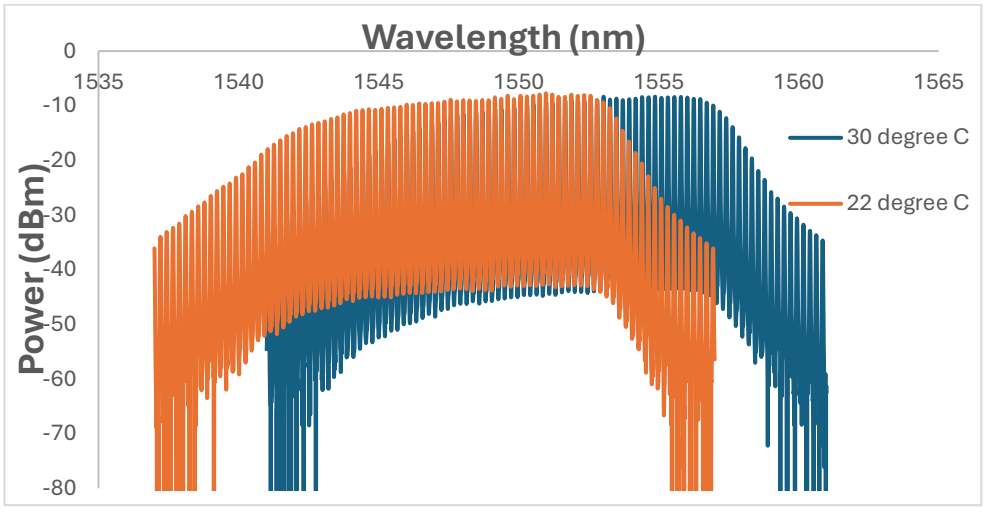


Figure 3.9 Optical spectrum measurement at 350mA for 22°$\boldsymbol{C}$ and 30°$\boldsymbol{C}$

### 3.4.3. RF spectra measurements of optical combs

This test is used to determine the repetition rate of the QDash device. Figure 3.10 shows the schematic of the experimental setup. Here the 90% output of the coupler is given to the RF signal analyzer via the optical attenuator. Optical attenuator is used because of the limitation of the input power given to the RF signal analyzer.

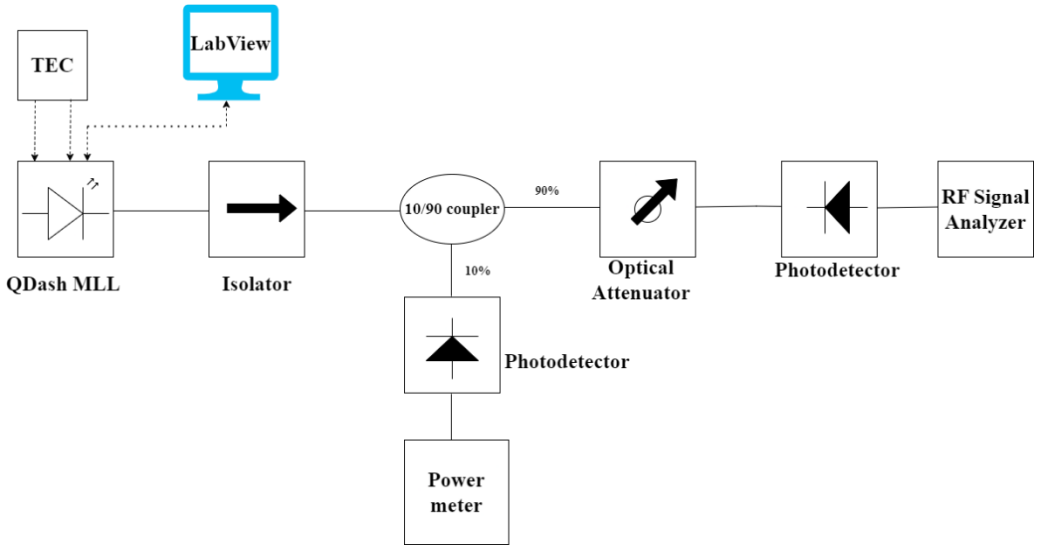


Figure 3.10 Experimental setup for RF measurement

The test was performed at 25°$C$ and the current was set at 90 mA which is well above the threshold current of 54mA for 25°$C$ from L-I measurements. The position of the sample is optimized to get maximum power by varying the lens position (lens is attached to the optical fibre that collects the output power from the QDash device) which capture the laser output power by observing the values in the power meter. Figure 3.11 shows the output RF spectra in a 400 MHz span from the signal analyzer. The beat frequency in this case is found to be 28.32 GHz corresponding to the peak power of -37.47 dBm. Multiple side peaks are observed along with the centre peak. To further analyse the side peaks, RF spectrum was measured by varying the position of lens (which capture the laser output) with respect to the sample. It was observed that when the lens position is away from the optimized position (i.e. maximum power position) a sharp single peak frequency is observed in the RF spectrum with narrow linewidth. It is also observed that there is a frequency shift towards the higher side in the non-optimized position and the peak power is more in case of non-optimized position. It is worthwhile to note that the peak power in case of non-optimized

position was more even though the total laser output was less because of the non-optimization of lens position. The comparison of RF spectrum between the optimized and non-optimized position of lens with respect to the QDash device is presented in Figure 3.12 and Table 3.3.

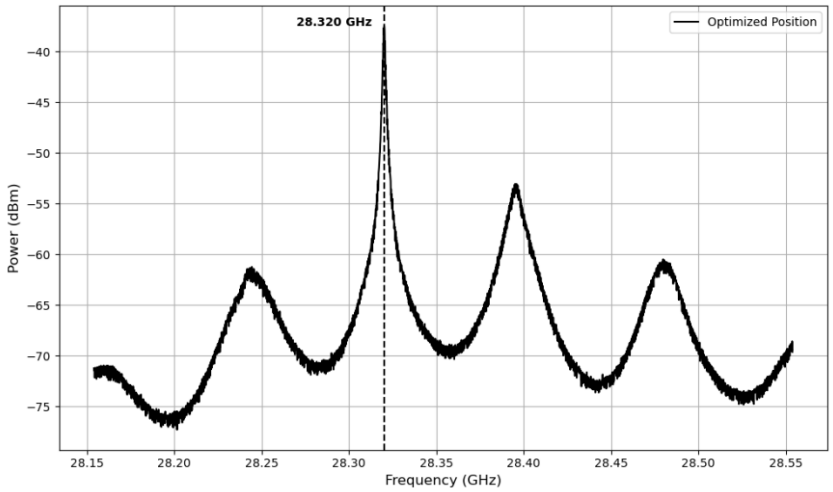


Figure 3.11 RF spectrum for 25°$\boldsymbol{C}$ at 90mA bias current optimized position

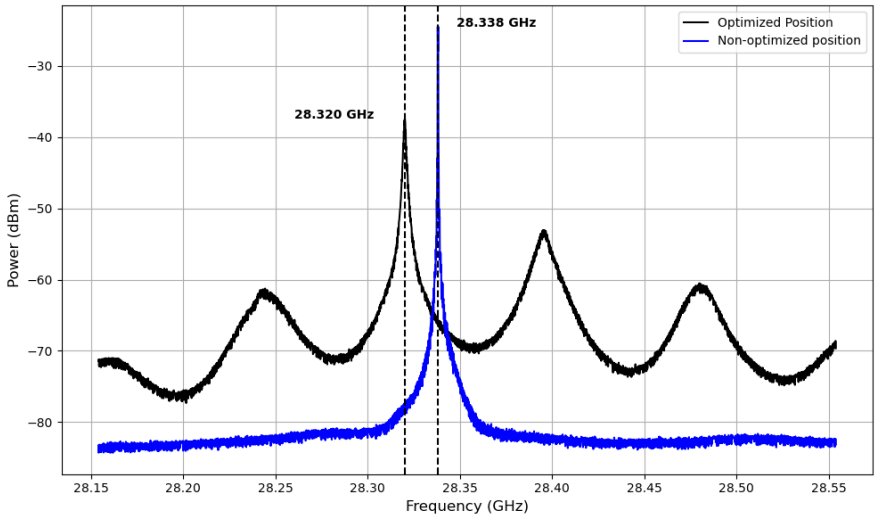


Figure 3.12 RF spectra for 25°$\boldsymbol{C}$ at 90mA bias current for optimized & non-optimized position

| **Parameters** | **Optimized position** | **Non-optimized position** |
|---|---|---|
| **Centre frequency (GHz)** | 28.320 | 28.338 |
| **Peak Power (dBm)** | -37.47 | -24.52 |
| **3 dB bandwidth (MHz)** | 1.22 | 0.13 |

Table 3.3 Comparison of parameters between optimized and non-optimized position of lens

RF spectrum was measured at optimized position for various bias current, and the results are presented in Figure 3.13. It is observed that the number of peaks seem to reduce as the bias current increases. There is also a frequency shift towards the higher side as we increase the current. The beat frequency observed at 60 mA is 28.318 GHz and whereas the beat frequency at 350 mA is 28.352 GHz. Thus, there is a frequency shift of 34 MHz from 60 mA to 350 mA bias current. Table 3.4 tabulates the peak frequency and power for different bias currents.

| **Bias Current (mA)** | **RF peak frequency (GHz)** | **Peak power (dBm)** |
|---|---|---|
| 60 | 28.318 | -59.7914 |
| 100 | 28.322 | -41.0555 |
| 150 | 28.328 | -47.2407 |
| 200 | 28.339 | -51.3780 |
| 250 | 28.343 | -48.0578 |
| 300 | 28.356 | -43.9769 |
| 350 | 28.352 | -31.6546 |

Table 3.4 RF peak frequency and power for different bias current

The side peaks observed could be due to back reflections and/or presence of higher transverse modes and/or due to fluctuations of pulse energy. Various studies have shown that with the use optical feedback loop there is an improvement of linewidth of RF spectrum and suppression of sidebands. Further analysis of this peculiar observation can be confirmed by experiments which involve observing the optical field and finding out the origin of back reflections (if present) from optical instruments/laser cavity etc. This was not considered in the scope of our thesis.

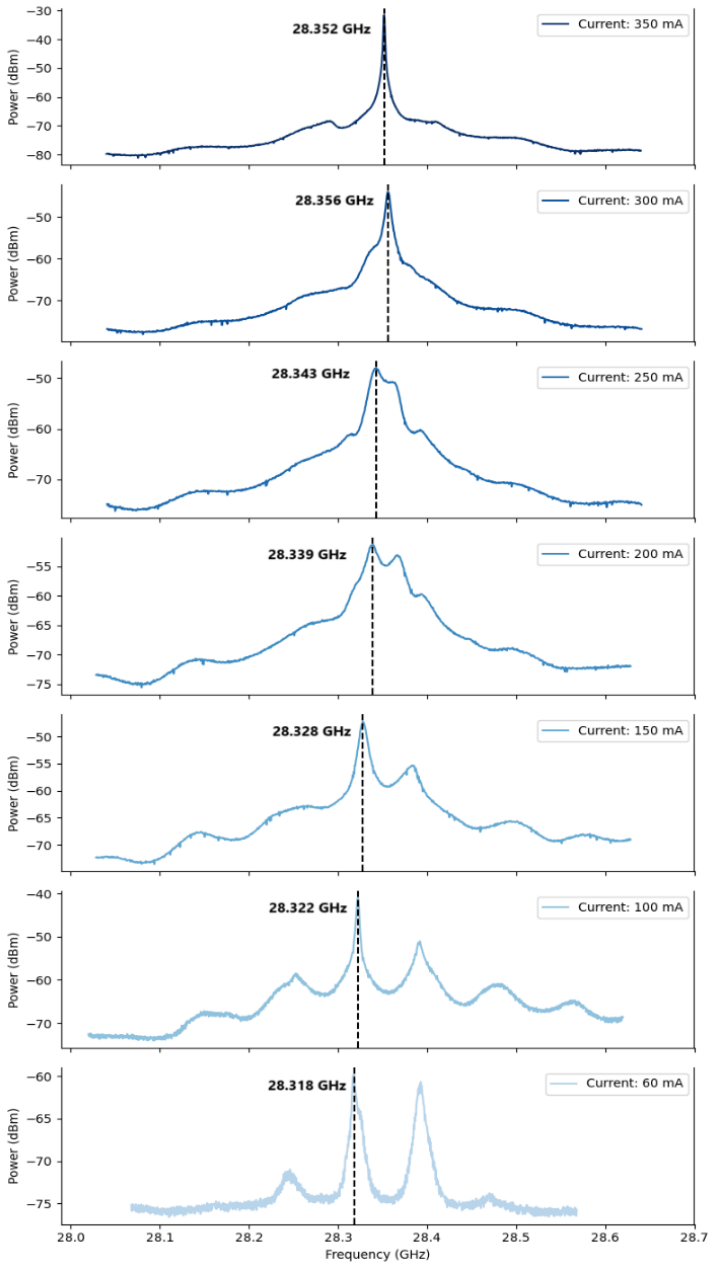


Figure 3.13 RF spectra for different bias current at 25°$C$

## 3.5. Dispersion

One of the important parameters that impacts the device performance is dispersion. Dispersion is a fundamental property of wave propagation where the velocity of light varies depending on it's wavelength or frequency. This causes different wavelength components to propagate at different times causing broadening of the of the pulses. It is important to study dispersion for optimizing optical systems as it directly impacts the efficiency and reliability of the system.

Dispersion can be expressed as the change in group delay with respect to wavelength. Group delay $\tau$ is the time taken for the envelope of an optical pulse to travel through a medium. For an optical medium of length 2L, group delay is,

$$\tau = \frac{2L}{v_g} \tag{3.1}$$

where $v_g = \frac{c}{n_g}$ is the group velocity and $n_g$ is the group refractive index. Hence the group delay per unit length is,

$$\tau = \frac{2Ln_g}{c} \tag{3.2}$$

Now, the dispersion is the rate of change of group delay with respect to wavelength,

$$D = \frac{d\tau}{d\lambda} = \frac{d}{d\lambda}\left(\frac{2Ln_g}{c}\right)$$
$$= \left(\frac{2L}{c}\right)\frac{dn_g}{d\lambda}$$

Using finite difference,

$$D = \frac{2L}{c}\,\frac{n_{g1} - n_{g2}}{\lambda_1 - \lambda_2} \tag{3.3}$$

This is the expression for material dispersion which is due to the change in refractive index of the material with respect to wavelength and is intrinsic to the material. The group refractive index can be found if we know the line spacing/frequency spacing between adjacent modes by using the formula,

$$\Delta\nu = \frac{c}{2n_g(\lambda)L} \tag{3.4}$$

where $\Delta\nu$ is the frequency spacing between adjacent modes.

### 3.5.1. Experiments to determine dispersion

Experiments are carried out to find dispersion of the material at different temperatures. Figure 3.14 shows the experimental setup to determine dispersion and the setup is similar to the one described in section 3.3.2. Temperature and current are set from the TEC controller and the current is set such that it is 5mA below the threshold current for the corresponding temperature obtained from the L-I measurements. Since the current is below the lasing condition, we obtain spontaneous emission spectrum observed in the optical spectrum analyzer. Dispersion calculated from this method gives us the material dispersion of the gain medium primarily due to the intrinsic properties of the material without the influence of lasing characteristics such as coherence feedback. The emission spectrum is analyzed and the line spacing between adjacent modes is found.

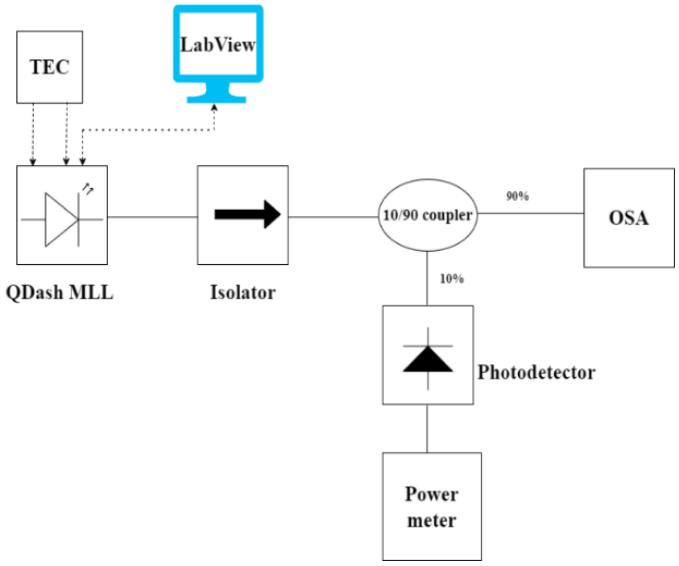


Figure 3.14 Experimental setup to determine dispersion

Experiments were carried out at four different temperatures $20°C$, $25°C$, $35°C$ and $45°C$. Figure 3.15 shows the emission spectra for these four temperatures for the wavelength range from 1540 nm to 1541.2 nm. Similarly, the emission spectra for higher wavelength for range between 1605 nm to 1606.2 nm is recorded. The line spacing is calculated by taking the difference between the adjacent peaks. The group refractive index is calculated using the linespacing values and corresponding wavelength with the help of equation 3.4. Table 3.5 shows the linespacing value for different temperatures and the corresponding calculated group refractive index. Figure 3.16 shows the plot between the group refractive index and temperature. It is observed that as temperature increases the group refractive index also increases.

| Temperature | Wavelength (nm) | Linespacing (nm) | Group R.I ($n_g$) |
|---|---|---|---|
| 20°$C$ | 1540.64 | 0.19755 | 3.548479 |
| | 1605.6 | 0.2178 | 3.495666 |
| 25°$C$ | 1540.6 | 0.1974 | 3.550959 |
| | 1605.6 | 0.2176 | 3.498879 |
| 35°$C$ | 1541.5 | 0.1975 | 3.553309 |
| | 1605.6 | 0.2171 | 3.5065 |
| 45°$C$ | 1540.6 | 0.1973 | 3.552759 |
| | 1605.6 | 0.2168 | 3.51179 |

Table 3.5 Linespacing and $n_g$ for different temperatures

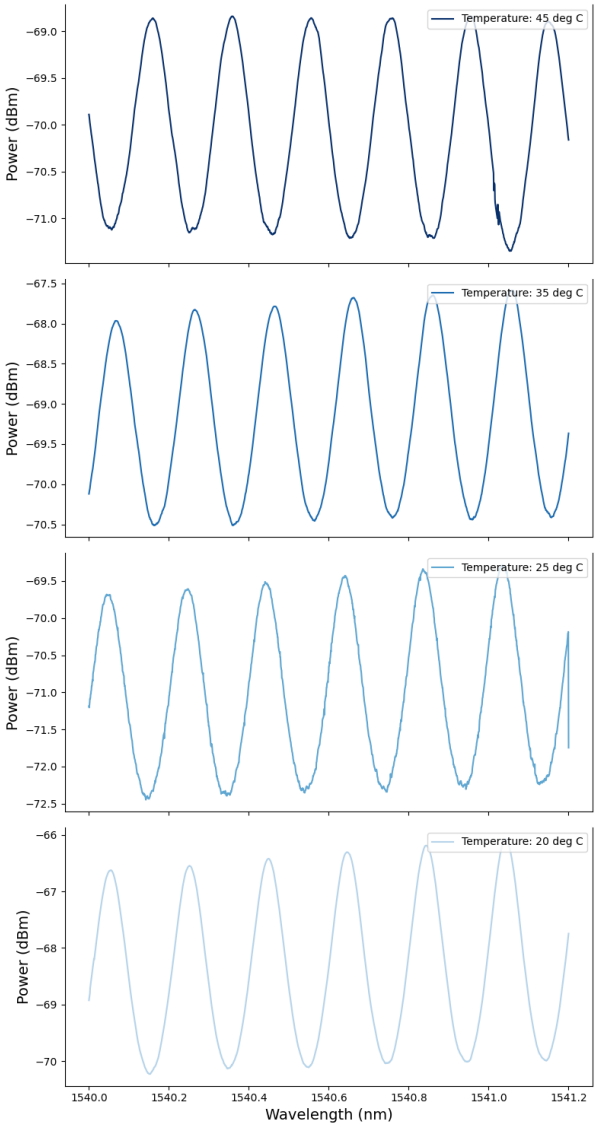


Figure 3.15 Emission spectra for different temperatures at currents 5mA below threshold

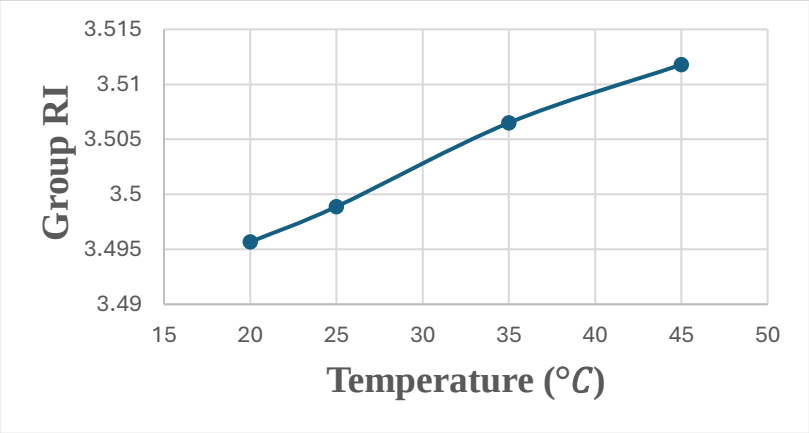


Figure 3.16 Variation of Group R.I ($n_g$) with respect to temperature

The dispersion values are calculated using the group refractive index as discussed in Section 3.5 and their values are tabulated in Table 3.6 and the corresponding plot is shown in Figure 3.16.

| Temperature | Dispersion (ps/nm) |
|---|---|
| 20°C | 0.00917 |
| 25°C | 0.00904 |
| 35°C | 0.00825 |
| 45°C | 0.00711 |

Table 3.6 Dispersion for different temperatures

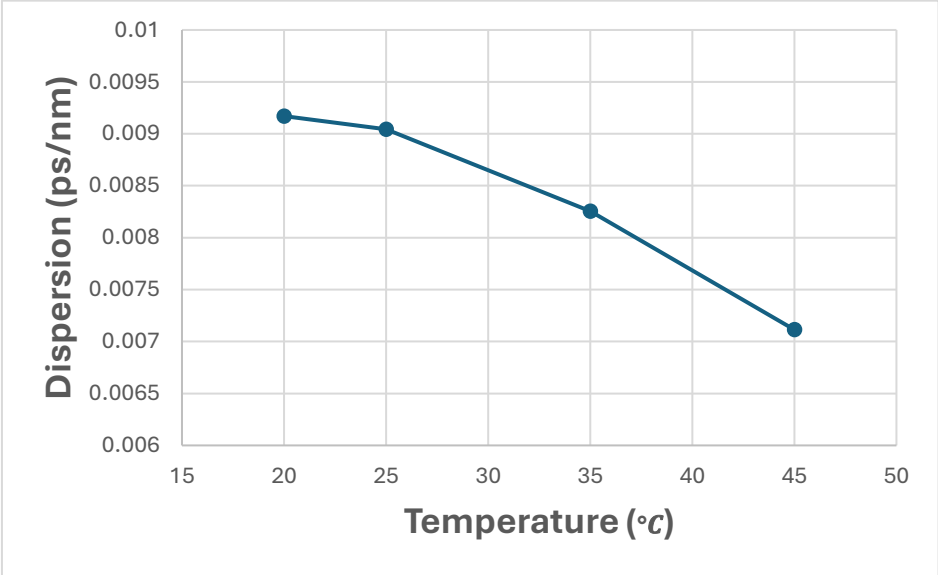


Figure 3.17 Plot of dispersion vs temperature

It is observed from the results that the dispersion value decreases as the temperature increases. This information is essential because it impacts the performance of the device for various applications. Material dispersion can be reduced by optimizing the device design by having uniform QDash structure, use of external dispersion compensation techniques.

## 3.6. Summary

In this chapter, the use of passive mode locked QDash laser for OFC generation is discussed. The density of states as a function of dimension of carrier movement is discussed and it has been realised that as the number of dimensions for carrier movement is reduced, the lasing efficiency is increased. Experiments were conducted on passive mode locked QDash laser to study the mode-locking characteristics. The L-I measurements carried out on the sample for different temperatures show that threshold current increases with the increase in temperature. It is also observed that with increase in temperature the optical spectrum shift towards the longer wavelength of the spectrum. Experimental measurements revealed that with increase in bias current, the spectral bandwidth is broadened generating more number of combs. The RF spectra measurements is carried out to find the repetition rate of the device. The repetition rate was found to be ~28.3 GHz and there is a frequency shift of 34MHz for bias current from 60 mA to 350 mA. Dispersion which is a critical parameter of wave propagation is studied as it directly impacts the reliability of the system. An expression for dispersion is derived which is used to calculate the dispersion values from experimental measurements for different temperatures. Based on the results, it is found that material dispersion of the device decreases slightly with increase in temperature. These findings provide valuable insights into optimizing QDash laser. This chapter highlights the potential of QDash laser for efficient OFC generation and its application in advanced optical communication.

# Chapter 4 OFC generation using fibre loop modulation technique

## 4.1. Introduction

Recent developments in OFC generation using electro-optic modulation is gaining momentum due to the numerous advantages offered by them. OFC generated using electro-optic modulation called the electro-optic combs (EOC) are highly tunable and their repetition rate can be changed without modifying the setup. The on-chip integration is also easy compared to MLL based OFC. These features prove advantageous in optical communication using OFC. In this chapter we shall see the principle of OFC generation using fibre loop modulation setup based on electro-optic effect exploited in a cavity. Simulations results are presented which is validated with experimental results. We shall also see the characteristics of the OFC and how we can change the comb characteristics without modifying the set up.

## 4.2. Principle of OFC generation

The principle of OFC generation involves exploitation of electro-optic effect in a cavity. Figure 4.1 shows the setup to generate EOC using fibre loop modulation technique. An input CW laser is phase modulated using dual drive MZM. The MZM is driven by RF signal given to the two arms. Optical amplifier is used in the loop to compensate for the loss of coupler and the modulator. As the modulated signal continually passes through the modulator in the fibre loop, a comb like spectrum is generated. The MZM together with the fibre loop forms the electro-optic cavity. Hence the electro-optic effect happens inside the fibred cavity. The phases of the signal emitted from the intracavity are actively mode locked using the modulator in the cavity. The setup is kept in resonant condition by actively enslaving the cavity.

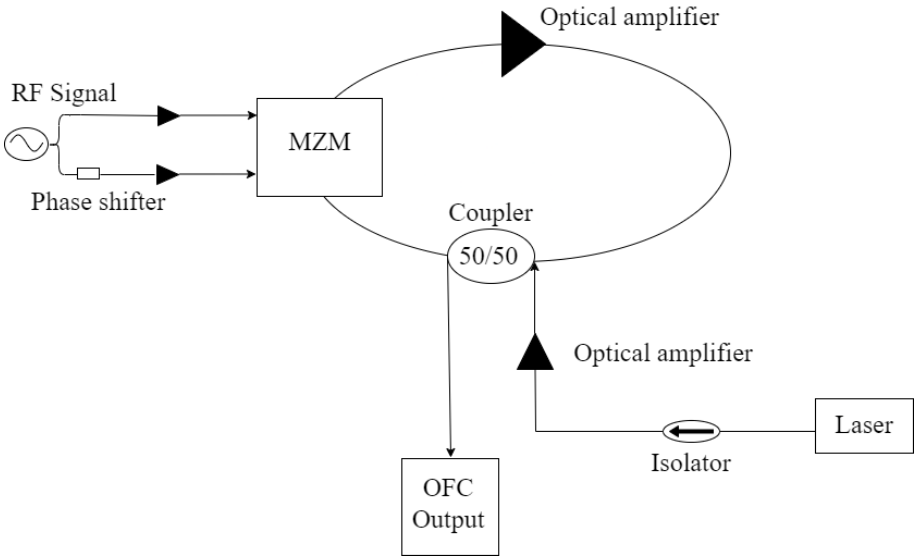


Figure 4.1 OFC generation using fibre loop modulation

Now, lets mathematically analyze the OFC generation using this method. The output signal from the modulator can be expressed as

$$E_{out}(t) = E_{in}(t)e^{j\phi} \tag{4.1}$$

where $E_{out}(t)$ is the output signal, $E_{in}(t)$ is the input signal and $\phi$ is the phase change of the signal introduced by the MZM. $E_{in}(t)$ can be expressed as

$$E_{in}(t) = E_o e^{j(2\pi f_o t + \phi_o)} \tag{4.2}$$

where $E_0(t)$ is the amplitude of the input signal, $f_o$ is the input (carrier) frequency, $\phi_o$ is the initial phase of the input signal.

The applied RF modulation signal can be expressed as

$$V_m(t) = V_{mo} \cos(2\pi f_{mo} t + \phi_{mo}) \tag{4.3}$$

where $V_{mo}$ is the amplitude of the modulation signal, $f_{mo}$ is the frequency of the modulation signal, $\phi_{mo}$ is the initial phase of the modulation signal.

The phase shift $\phi$ introduced by MZM through opto-electric effect is directly proportional to the applied voltage. Hence to introduce a phase shift of $\pi$, lets consider the applied voltage required as $V_\pi$. Therefore,

$$\phi = \pi\left(\frac{V_m(t)}{V_\pi}\right) \tag{4.4}$$

Combining all the above equations, $E_{out}(t)$ can be expressed as,

$$E_{out}(t) = E_{in}(t)e^{j\pi\left(\frac{V_m(t)}{V_\pi}\right)}$$

$$E_{out}(t) = E_{in}(t)e^{j\pi\left(\frac{V_{mo}\cos(2\pi f_{mo}t+\phi_{mo})}{V_\pi}\right)} \tag{4.5}$$

Using Jacobi-Anger expansion,

$$e^{izcos\theta} = J_o(z) + 2\sum_{n=1}^{\infty} i^n J_n(z)\cos(n\theta)$$

where $J_n(z)$ are the n-th Bessel functions of the first kind and z is the modulation index. In our case $z = \pi\left(\frac{V_{mo}}{V_\pi}\right)$

Hence, applying Jacobi-Anger expansion,

$$e^{j(\frac{\pi V_{mo}}{V_\pi}\cos(2\pi f_{mo}t+\phi_{mo})} = J_o\left(\frac{\pi V_{mo}}{V_\pi}\right) + 2\sum_{n=1}^{\infty} j^n J_n\left(\frac{\pi V_{mo}}{V_\pi}\right)\cos\big(n(2\pi f_{mo}t + \phi_{mo})\big)$$

Now,

$$E_{out}(t) = E_{in}(t)\left[J_o\left(\frac{\pi V_{mo}}{V_\pi}\right) + 2\sum_{n=1}^{\infty} j^n J_n\left(\frac{\pi V_{mo}}{V_\pi}\right)cos\big(n(2\pi f_{mo}t + \phi_{mo})\big)\right]$$

$$E_{out}(t) = E_o e^{j(2\pi f_o t+\phi_o)}\left[J_o\left(\frac{\pi V_{mo}}{V_\pi}\right) + 2\sum_{n=1}^{\infty} j^n J_n\left(\frac{\pi V_{mo}}{V_\pi}\right)cos\big(n(2\pi f_{mo}t + \phi_{mo})\big)\right]$$

Using trigonometric identity $\cos(n\theta) = \frac{1}{2}(e^{jn\theta} + e^{-jn\theta})$ where $\theta = 2\pi f_{mo}t + \phi_{mo}$,

$$E_{out}(t) = E_o e^{j(2\pi f_o t+\phi_o)}\left[J_o\left(\frac{\pi V_{mo}}{V_\pi}\right) + \sum_{n=1}^{\infty} j^n J_n\left(\frac{\pi V_{mo}}{V_\pi}\right)(e^{j[n(2\pi f_{mo}t+\phi_{mo})]} + e^{-j[n(2\pi f_{mo}t+\phi_{mo})]})\right]$$

$$E_{out}(t) = E_o \left[ J_o\left(\frac{\pi V_{mo}}{V_\pi}\right) e^{j(2\pi f_o t + \phi_o)} + \sum_{n=1}^{\infty} j^n J_n\left(\frac{\pi V_{mo}}{V_\pi}\right) (e^{j[n(2\pi f_{mo} t + \phi_{mo})]} e^{j(2\pi f_o t + \phi_o)} + e^{-j[n(2\pi f_{mo} t + \phi_{mo})]}) e^{j(2\pi f_o t + \phi_o)} \right]$$

$$E_{out}(t) = E_o \left[ J_o\left(\frac{\pi V_{mo}}{V_\pi}\right) e^{j(2\pi f_o t + \phi_o)} + \sum_{n=1}^{\infty} j^n J_n\left(\frac{\pi V_{mo}}{V_\pi}\right) (e^{j[2\pi(f_o + n f_{mo})t + n\phi_{mo} + \phi_o]} + e^{j[2\pi(f_o - n f_{mo})t - n\phi_{mo} + \phi_o]} \right]$$

Using Euler's formula for the exponential terms and considering the real part we get,

$$E_{out}(t) = E_o \left\{ J_o\left(\frac{\pi V_{mo}}{V_\pi}\right) \cos(2\pi f_o t + \phi_o) + \sum_{n=1}^{\infty} (-1)^n J_n\left(\frac{\pi V_{mo}}{V_\pi}\right) [\cos(2\pi(f_o + n f_{mo})t + n\phi_{mo} + \phi_o) + \cos(2\pi(f_o - n f_{mo})t - n\phi_{mo} + \phi_o)] \right\}$$

From the last expression we observe that the output signal is a frequency spectrum containing the original carrier frequency $f_o$ and sidebands spaced by integer multiples of the modulation frequency $f_{mo}$. Thus, the interval between the adjacent sidebands of the frequency spectrum is directly dependent on the frequency of the RF modulational signal. The amplitude of the sidebands is symmetrically distributed on either side of the centre carrier frequency and obey the Bessel function of different orders.

## 4.3. Numerical simulations of OFC generation

Numerical simulations of OFC generation by fibre loop modulation technique was performed using the commercially available software – OptiSystem. The setup for the simulation is identical to the one described in Section 4.2. A CW laser of 1532nm having power 10 dBm was injected into the fibre loop through the 50/50 coupler via an isolator. The isolator is used to ensure the signal is transmitted in one direction. The circulating signal was modulated by a 50 GHz RF signal having amplitude of 9 V in each round trip. Optical amplifier is used in the loop to compensate for the loss of coupler and the modulator. Half of the optical signal in the loop is extracted by the

output of the coupler resulting in an OFC. Figure 4.2 shows the simulated OFC, and it is observed that 89 number of comb lines with ~ 6dB flatness are generated.

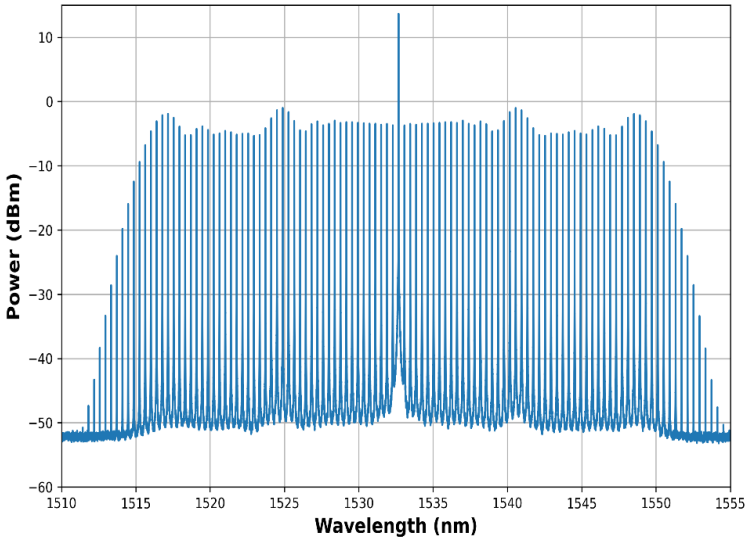


(a)

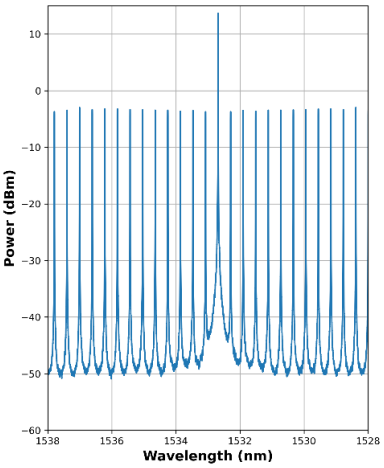


(b)

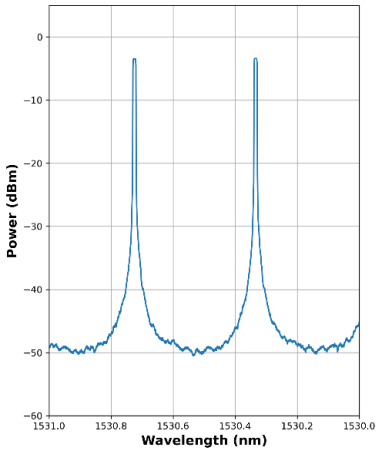


(c)

Figure 4.2 Simulation result of OFC showing (a) full OFC spectrum (b) narrow spectrum to show the flatness of the combs (c) two adjacent combs

44 number of comb lines on either side of the centre comb was generated with linespacing between the adjacent comb as 50 GHz which is equal to the frequency of the RF modulation signal. The bandwidth of the generated OFC is 4.4 THz. The centre wavelength of the comb is 1532 nm, which is equal to the wavelength of the input laser. We also observe that the centre comb line amplitude is higher than the combs of sidebands. This could be due to the limitation of the maximum RF signal given to the modulator resulting in lower power per OFC line generated.

## 4.4. Characteristics of combs

From the mathematically analysis of OFC generation using phase modulator, we observed that the frequency of comb was dependent on the RF modulation signal. Simulations were carried out to study the comb line characteristics with respect to RF signal. The amplitude of the RF signal was incremented in steps and the number of comb lines generated for each case was recorded. Table 4.1 shows the number of comb lines generated and the corresponding amplitude of the RF signal used. It is observed that as the RF signal increases the number of comb lines generated in the OFC also increase. Figure 4.3 shows the plot between RF amplitude and the corresponding number of combs generated in the OFC. It is observed that the relation between the amplitude of RF signal and the number of combs is approximately linear. Figure 4.4 shows the simulated OFC for different amplitude of the RF signal.

| **Amplitude of RF signal (V)** | **Number of comb lines generated** |
|---|---|
| 1 | 11 |
| 3 | 33 |
| 5 | 51 |
| 7 | 69 |
| 9 | 89 |
| 11 | 109 |

Table 4.1 Amplitude of RF signal and corresponding number of combs in OFC

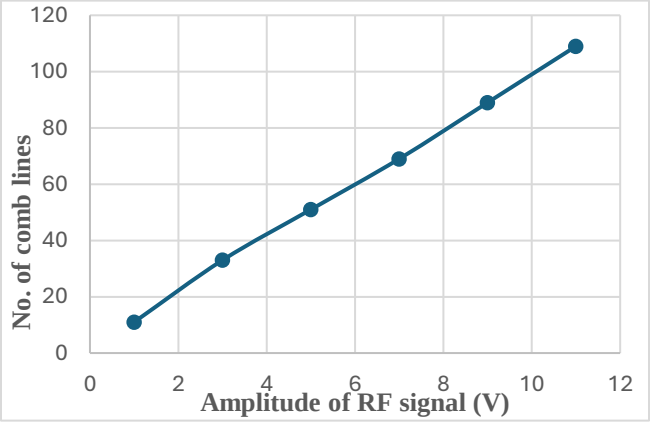


Figure 4.3 Comb line characteristics with respect to RF signal amplitude

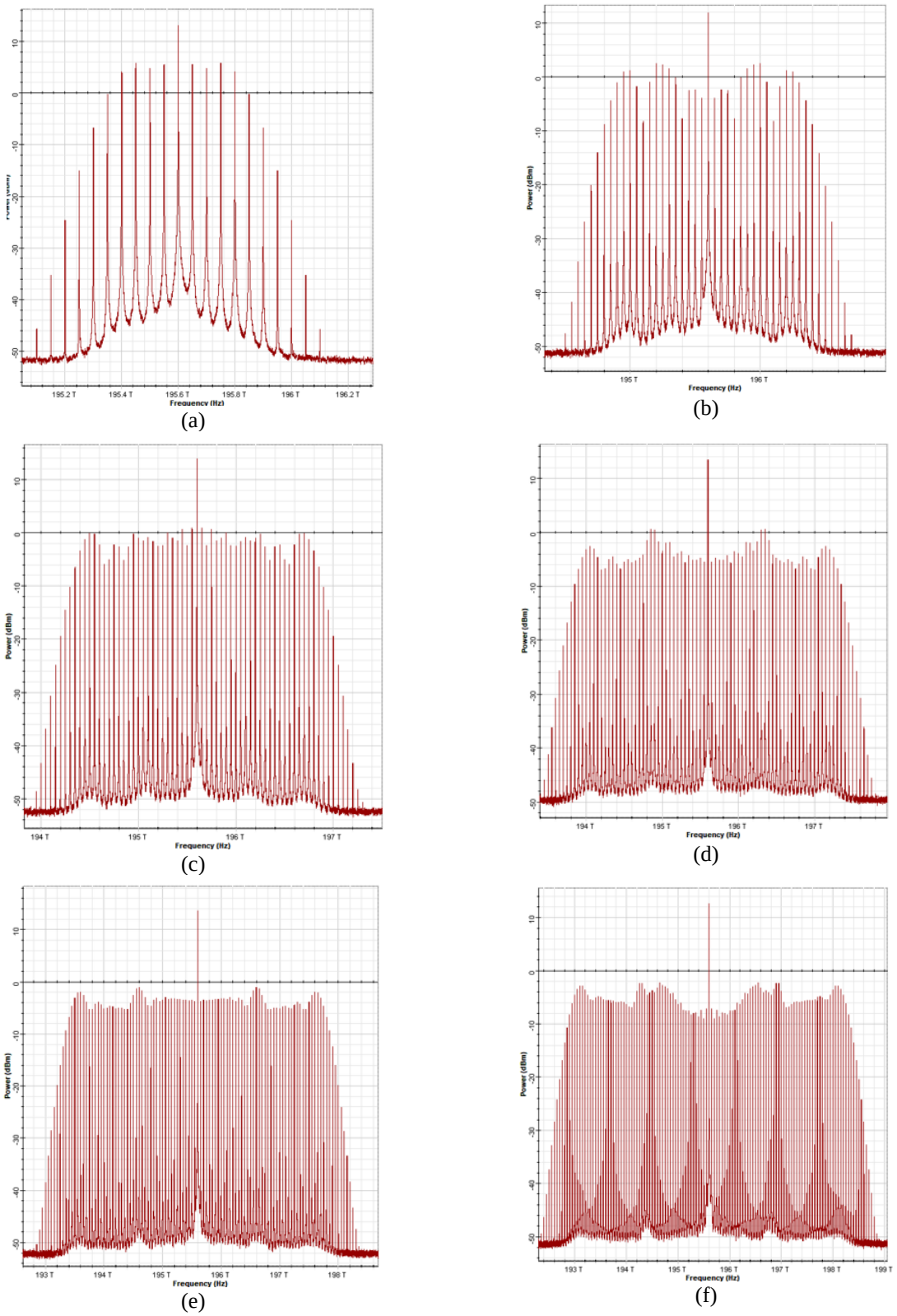


Figure 4.4 Simulated OFC for different RF amplitude (a) 1 V (b) 3 V (c) 5 V (d) 7 V (e) 9 V (f) 11 V

## 4.5. Experimental results

Experiments were carried out to generate OFC using the fibre loop modulation technique. The experiment was carried out and data was provided by our collaborator from School of Electronic Engineering, Dublin City University, Ireland. The experimental setup is same as the one described in Section 4.2. A CW laser of 1532 nm wavelength power was injected into the fibre loop. A RF modulating sinusoidal signal of 12 GHz with 1 V amplitude was given to the dual drive MZM which introduces phase modulation to the optical carrier from the laser. The new frequency components are generated by continually passing the signal in the loop and half of the optical signal output is taken out from the 50/50 coupler. Figure 4.5 shows the experimentally generated OFC. It is observed that a total of 34 comb lines are generated with 17 lines and 16 lines on the right and left side of the centre comb. The centre comb wavelength is ~1532 nm which is equal to the wavelength of the laser. The line spacing between the adjacent comb is found to be 12 GHz which is equal to the frequency of RF modulating signal.

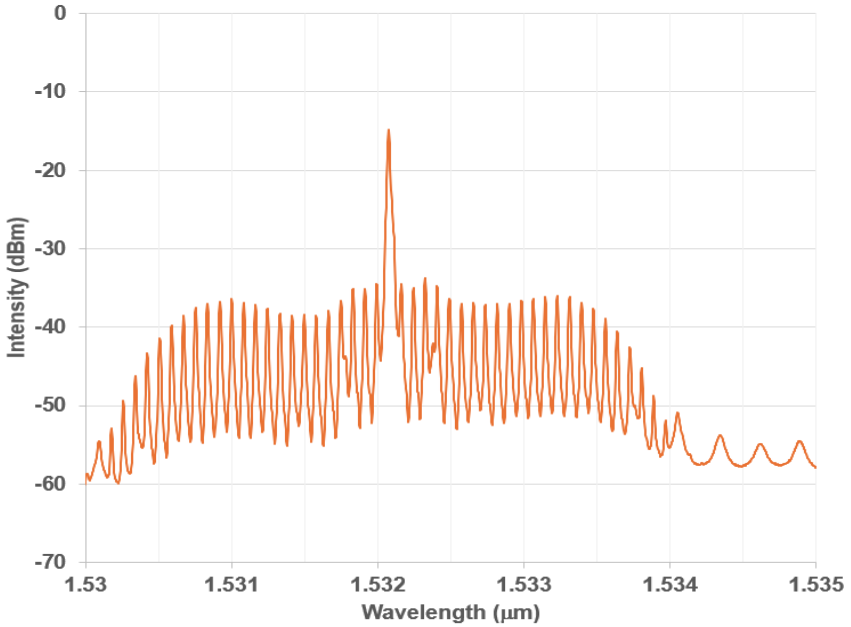


Figure 4.5 Experimentally generated OFC

## 4.6. Comparison of experimental and simulation results

Simulations were performed to validate the experimental results obtained in Section 4.5. The simulation conditions are tabulated in Table 4.2 which is same as the experimental conditions.

| Simulation parameters | Value |
|---|---|
| Input laser wavelength | 1532 nm |
| Input laser power | 10 dBm |
| RF modulating signal frequency | 12 GHz |
| RF signal amplitude | 1 V |

Table 4.2 Simulation input parameters

Figure 4.6 shows the simulation result of the OFC generation where the simulation parameters are the same as experiment. From the simulation results an OFC of 33 comb lines was generated with 16 lines on either side of the centre comb of wavelength 1532nm. Figure 4.7 shows the comparison between the OFC generation using simulation and experiment. A fitting factor of 20 dBm for amplitude and 0.21 nm for wavelength is used. We observe that a good agreement is obtained between experiment and simulation. Table 4.3 lists the output results of simulation and experiment.

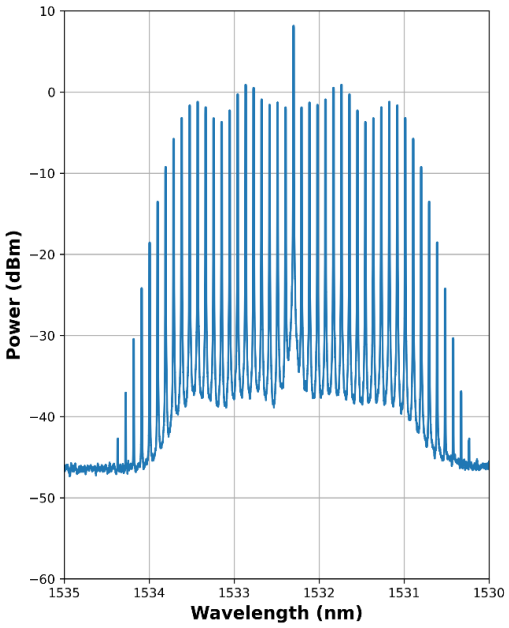


Figure 4.6 Simulation result of the generated OFC

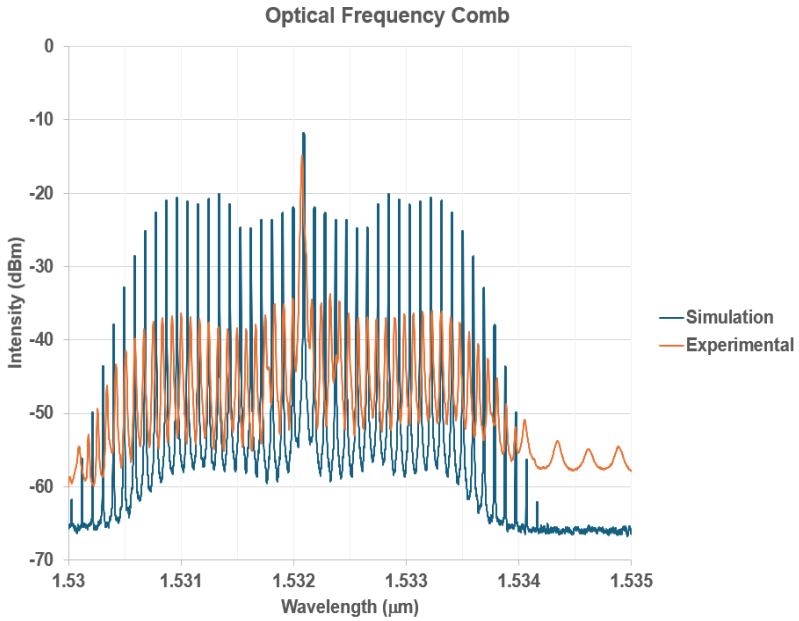


Figure 4.7 OFC generation comparison between simulation and experiment

| Output results | Simulation | Experiment |
|---|---|---|
| No. of comb lines generated | 33 | 34 |
| Centre comb length | 1532 nm | 1532 nm |
| Comb line spacing | 12 GHz | 12 GHz |

Table 4.3 Comparison of Simulation and Experiment results

The lower level of amplitude in experiment results compared to the simulation can be attributed to the loss in MZM and coupler. The fitting factor for wavelength used is due to the laser wavelength variation used in the experiment. We observe there is a considerable power difference between the centre comb and the sidebands in case of experiment as compared to the simulation results. This can be attributed to the loop loss being more in case of experiment as compared to the simulation.

## 4.7. Summary

This chapter delves into the OFC generation using fibre loop modulation technique which is based on the exploitation of electro-optic effect in a cavity. The principle of generation is explained and a mathematical expression is derived analyzing the OFC generation. An important conclusion from the expression is that the interval between the adjacent combs is equal to the frequency of the

modulating signal. Hence we see that the OFC can be modified by changing the frequency of the modulating signal thereby changing the repetition rate. This method proves advantageous as they are highly tunable without modifying the setup. Simulations were performed to generate OFC by this method using OptiSystem software. We were able to generate a broad optical spectrum containing 89 number of combs with ~6 dB flatness. The interval between the comb lines was 50 GHz which was equal to the frequency of the modulating signal, thus corroborating the derived mathematical expression. We also studied the effect of varying amplitude of the modulating signal on the comb characteristics. Based on the simulation results, it is observed that as the amplitude of RF signal increases the number of generated combs also increases further demonstrating the tunability of this method. Experiments were also conducted to validate the simulation results. An OFC with 33 number of comb lines was generated experimentally with a repetition rate of 12 GHz equal to the modulating signal frequency. Simulations under the same conditions as of experiment generated spectrum containing 34 number of comb lines with 12 GHz repetition rate. Hence a good agreement is obtained between experiment and simulation results. In conclusion this chapter demonstrates the effectiveness of the fibre loop modulation technique for generating OFCs.

# Chapter 5 OFC application in DWDM communication

## 5.1. Introduction to DWDM technology

Dense Wavelength Division Multiplexing (DWDM) is an advanced technology in optical communication which combines several signals running at different wavelengths and transmitting them within a single optical channel. It usually involves using a number of laser sources i.e. one laser source for each channel and transmitting them in a single optical fibre. Figure 5.1 shows the conventional DWDM system using individual laser source at different wavelengths as sources. All the individual laser sources are modulated and the multiplexed signal is transmitted through the single optical transmission medium. At the output the signal is demultiplexed and converted back to individual data signals.

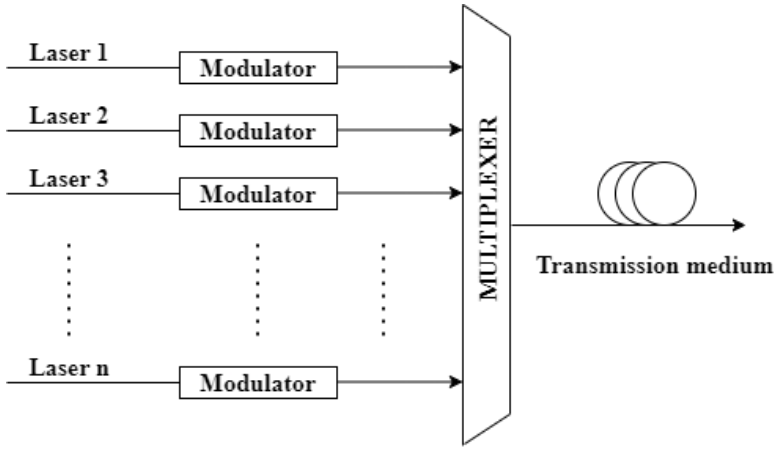


Figure 5.1 Conventional DWDM system using individual lasers as sources

DWDM enables efficient transmission of high-capacity data over long distance and are extremely scalable and cost effective. In this chapter we shall see the application of OFC in DWDM communication system and model a system where the optical transmission medium is free space.

## 5.2. Free space optical communication

Free space optical communication (FSO) is an emerging technology that addresses the last mile connectivity problem. FSO is a line-of-sight communication that uses optical spectrum to transmit signal through atmosphere. FSO when used as the transmission medium in DWDM system enable high-capacity data transmission without relying on optical fibre infrastructure thus reducing the

overall cost. FSO is particularly useful in urban networks bridging the gap between communication fibre network and end-users. They manage the backhaul solutions efficiently in remote areas supporting high speed data communication and IoT (Internet of things) networks. FSO offers seamless integration into DWDM system and can be deployed rapidly. They prove advantageous in establishing quick communication links during natural disasters and network outages. Even though FSO communication systems offers high speed and high-capacity data transmission, they have significant challenges. Some of these include the line-of-sight limitations and misalignment between the transmitter and receiver. Alignment between the transmitter and receiver is crucial as even small misalignments can degrade the signal to a great extent. While these challenges can be overcome by using improved beam technology, the main concern in FSO communication is the atmospheric conditions. Adverse weather conditions may degrade the signal quality by scattering and absorbing phenomenon in the atmosphere posing a barrier for reliable communication. Several approaches such as adaptive optics, careful selection of optical wavelength can help mitigate atmospheric interference. In the next section we shall see the wavelength dependence on the atmospheric attenuation in FSO system.

### 5.2.1. Wavelength dependence on atmospheric attenuation

The atmosphere consists of various particles which causes absorption and scattering resulting in attenuation of optical signal. It is known that signals at different wavelengths experience varying levels of attenuation in atmosphere. This can be better analysed by the Beer-Lambert law. It describes the attenuation of light as it travels through a medium and is expressed as,

$$T\ (\lambda) = \frac{P_d}{P_o} = e^{-\sigma d} \tag{5.1}$$

where $T\ (\lambda)$ is transmittance at wavelength $\lambda$ which represents the fraction of light ($P_d$ ) received at a distance d to the total light at source ($P_o$ ) and $\sigma$ is the attenuation coefficient.
The attenuation $\alpha$ (dB/km) can be found using the following equation,

$$\alpha = \frac{10\log\left(T\ (\lambda)\right)}{d} = -10\log e\ (\sigma) \tag{5.2}$$

In FSO communication system the attenuation can be due to different scattering effects. The main scattering effects are Rayleigh and Mie scattering. Mie scattering is more significant in the generally used communication wavelength which lies in the infrared spectrum. The attenuation coefficient for Mie scattering of a particular wavelength of light $\lambda$ can be determined by equation 5.3 and it is related to the visibility of the weather conditions V.

$$\sigma = \frac{3.91}{V}\left(\frac{\lambda}{550}\right)^{-q} \tag{5.3}$$

where $q$ is size distribution of scattering particles which can be determined by the Kim model. Equation 5.4 shows the values of $q$ for varying visibility

$$q = \begin{cases} 1.6 & V \geq 50\ km \\ 1.3 & 6\ km \leq V < 50\ km \\ 0.16V + 0.34 & 1\ km \leq V < 6\ km \\ V - 0.5 & 0.5\ km \leq V < 1\ km \\ 0 & V < 0.5\ km \end{cases} \tag{5.4}$$

Simulations were carried in OptiSystem software out to find the attenuation for two different wavelengths of 785 nm and 1550 nm and verify the wavelength dependence. Table 5.1 shows the simulation results for attenuation values for these two wavelengths for various visibility ranges and Figure 5.2 shows the plot between them.

| **Visibility (km)** | **Attenuation for 785 nm (dB/km)** | **Attenuation for 1550 nm (dB/km)** |
|---|---|---|
| 0.05 | 339.794 | 339.794 |
| 0.2 | 84.94 | 84.94 |
| 0.5 | 33.97 | 33.97 |
| 1 | 14.22 | 10.12 |
| 2 | 6.717 | 4.28 |
| 4 | 2.99 | 1.53 |

| | | |
|---|---|---|
| 10 | 1.0698 | 0.4418 |
| 23 | 0.465 | 0.192 |

Table 5.1 Attenuation values for 785 nm and 1550 nm wavelengths for different visibility ranges

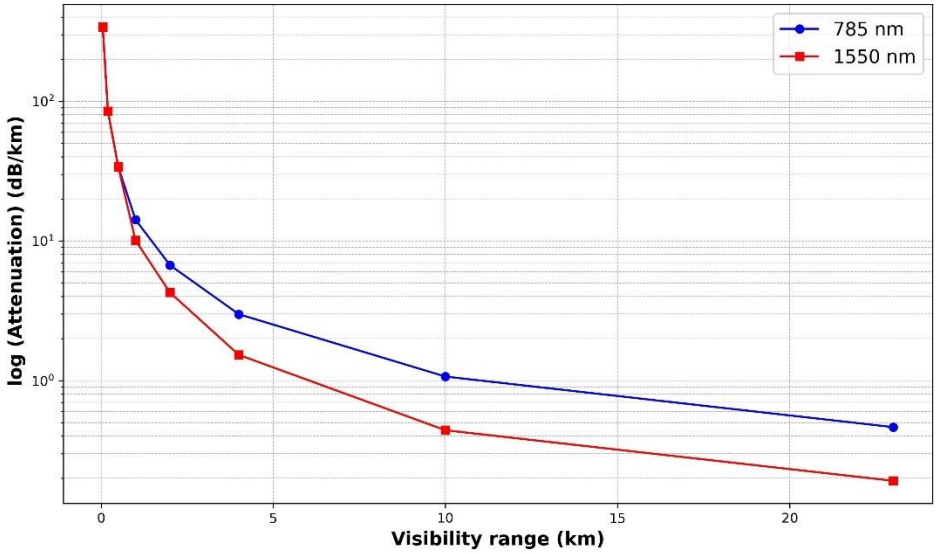


Figure 5.2 Plot between attenuation and visibility range for 785 nm and 1550 nm wavelength

It is seen from the results that the attenuation values remain the same for different wavelengths under low visibility ranges up to 0.5 km. When the visibility range increases the shorter wavelength light undergoes more attenuation that the longer wavelength. It should be noted that these results are for foggy conditions (Mie scattering) and does not consider the attenuation to adverse weather conditions like rain, snow, hail (geometrical scattering). This observation of wavelength independent attenuation for low visibility range in foggy conditions is important for practical purposes. Generally, 1550 nm wavelength is considered for free-space communication as it is less affected by weather. However, we have seen that there is no wavelength dependence in attenuation for low visibility range. Hence, different transmission wavelength can be utilised for shorter links especially to solve the last mile connectivity.

## 5.3. Transmission of OFC over FSO channel

We have seen in previous section that DWDM technology is capable of transmission of high-capacity data which requires individual laser sources for each channel. These individual laser

sources can be replaced by a single source of OFC thus revolutionising the field of optical networking. OFC which generates discrete equally spaced frequencies serve as a stable coherent source for multiple wavelength channels. Using OFC as a single source in DWDM communication offers many advantages such as reduction in energy consumption and system complexity, better spectral efficiency due to stable spacing. Multiple data links can be added making the system extremely scalable. They also allow precise channel spacing reducing crosstalk. Thus, the synergy between OFC technology and DWDM systems provides more efficient, scalable and flexible optical communication networks.

### 5.3.1. System Modelling and numerical simulations

Figure 5.3 shows the block diagram of a system for transmission of data over FSO channel using OFC source. We have considered an OFC source with 89 comb lines which is demultiplexed using 89-channel demultiplexer. Each output channel of the demultiplexer is modulated with 10 Gbps data using the non-return zero (NRZ) pulse format. 10 Gbps data is generated using the PRBSG (Pseudo random bit sequence generator) which is modulated with NRZ pulse generator to form electrical signal. The optical carriers are modulated with this signal and multiplexed using the multiplexer. The multiplexed signal is then transmitted over the free space optical channel. The attenuation in free space considered is 0.4 dB/km and the free space range is varied from 0.1 km to 1 km for analysis. At the receiver side, the transmitted signal is demultiplexed which is then followed by direct detection using photodetector. The signal is regenerated using the 3R regenerator and BER analyzer is placed to analyze the performance of the system.

Simulations were performed for the proposed system in OptiSystem software. 89 number of comb lines was generated using the fibre loop modulation technique. The various simulation conditions considered are presented in Table 5.2.

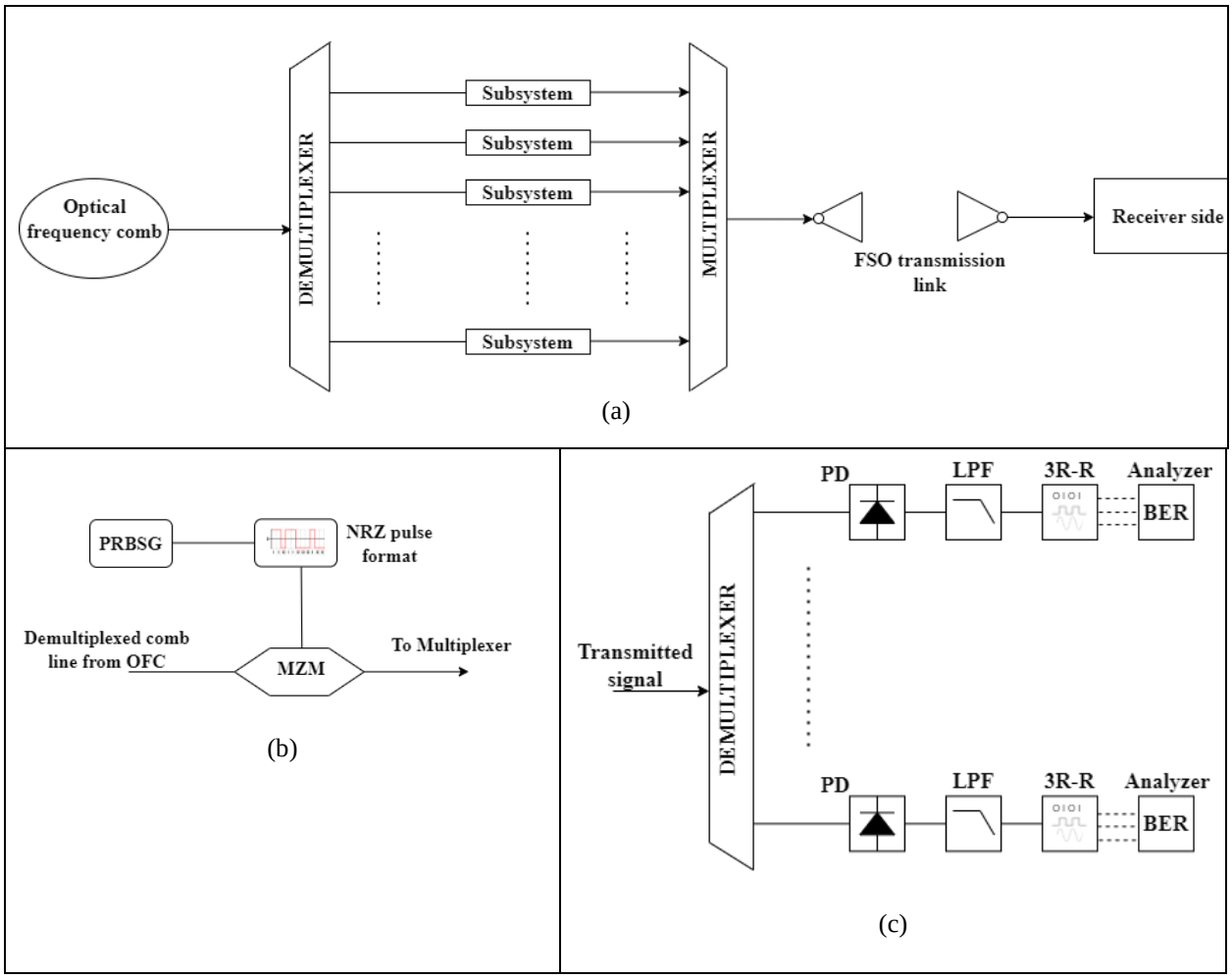


Figure 5.3 (a) Overall block diagram for data transmission over FSO, (b) Subsystem (part of overall block diagram), (c) Receiver side

| Input parameter | Value |
|---|---|
| Bit rate | 10 Gbps |
| Sequence length | 256 bits |
| Samples per bit | 1024 |
| Bandwidth of demultiplexer | 25 GHz |
| Bandwidth of multiplexer | 25 GHz |
| Data modulation scheme | NRZ |
| Attenuation of free space | 0.4 dB/km |
| Free space range | Varied from 0.1 km to 1 km |

Table 5.2 Input simulation parameters

## 5.4. Performance analysis of the proposed system

Performance analysis of the proposed system in terms of bit error rate (BER) and eye diagrams was done based on the simulation results. BER is an important metric in communication system to assess the quality of the received signal and reliability of the communication system. It is the ratio of number of bit error to the total number of transmitted bits. For example, a BER requirement of $10^{-4}$ means that out of $10^{4}$ transmitted bits, one error bit is permissible for satisfactory performance. Eye diagrams are a visualization tool that is used to evaluate signal quality and performance. It is created by superimposing multiple bits of a signal over a common time interval forming a pattern that resembles an eye. A wider and clear eye opening indicates that signal has less noise and interference. BER together with eye diagrams can help diagnose issues, troubleshooting and optimize system performance.

Simulations were performed for the proposed system keeping the range of FSO channel as 1 km and BER values for the individual output channels was recorded. Figure 5.4 shows the eye diagrams of the received signal for four output channels of the total 89 channels and their corresponding BER is tabulated in Table 5.3.

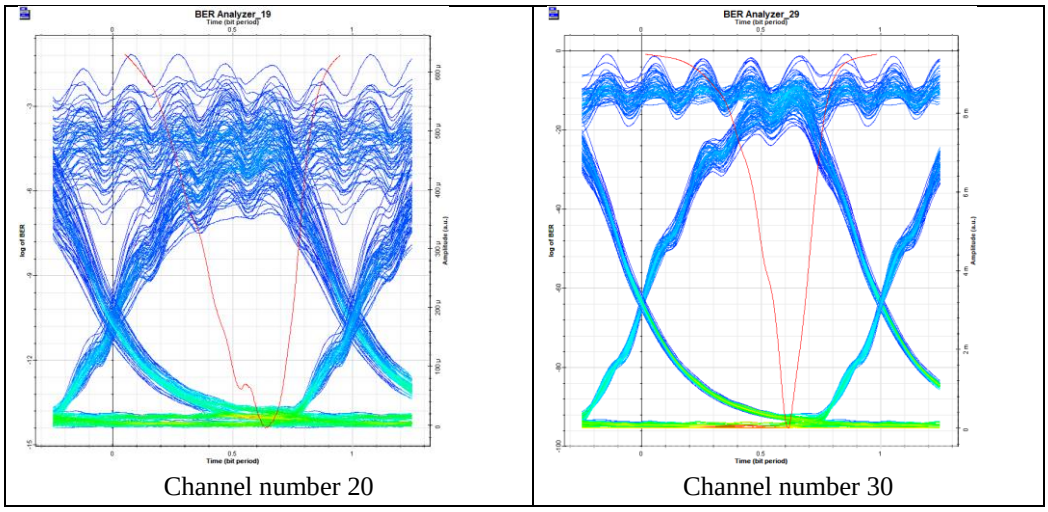


Channel number 20 | Channel number 30

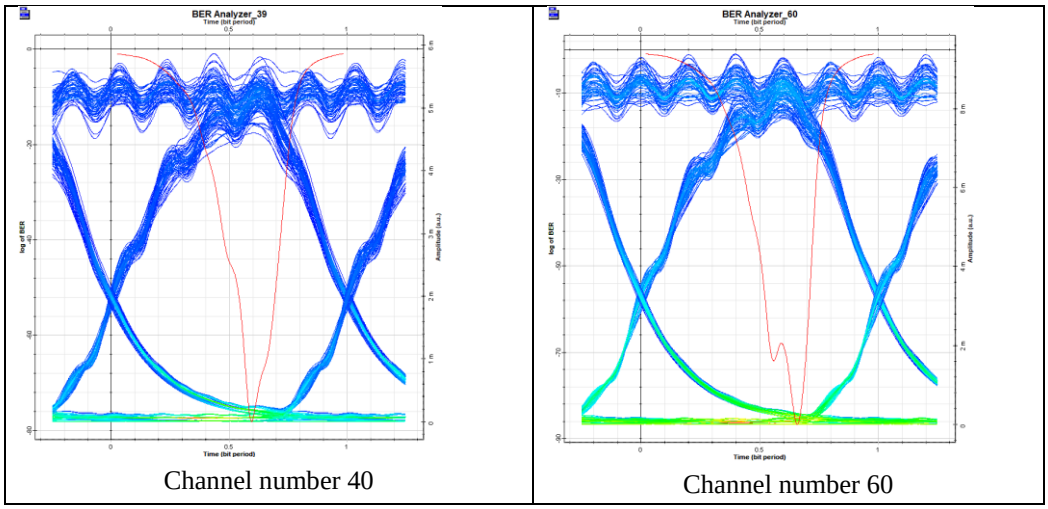


Channel number 40 Channel number 60

Figure 5.4 Eye diagrams for four of the 89 output channels

| Channel number | BER value |
|---|---|
| 20 | $3.98 \times 10^{-15}$ |
| 30 | $5.29 \times 10^{-96}$ |
| 40 | $7.91 \times 10^{-79}$ |
| 60 | $2.14 \times 10^{-87}$ |

Table 5.3 BER values for different output channels

We observe that the quality of received signals in most of the output channels are good based on the eye diagrams and BER values. The results presented in Table 5.3 is for free space range of 1 km suggesting that our system is capable for long distance.

Simulations were also performed by varying the range of FSO channel. The FSO channel range considered are 100 m, 500 m, 700 m and 1000m. In each case the BER values are recorded, and the corresponding eye diagrams are observed. Figure 5.5 shows eye diagrams for output channel number 40 for the four cases of FSO range. The corresponding BER values are presented in Table 5.4.

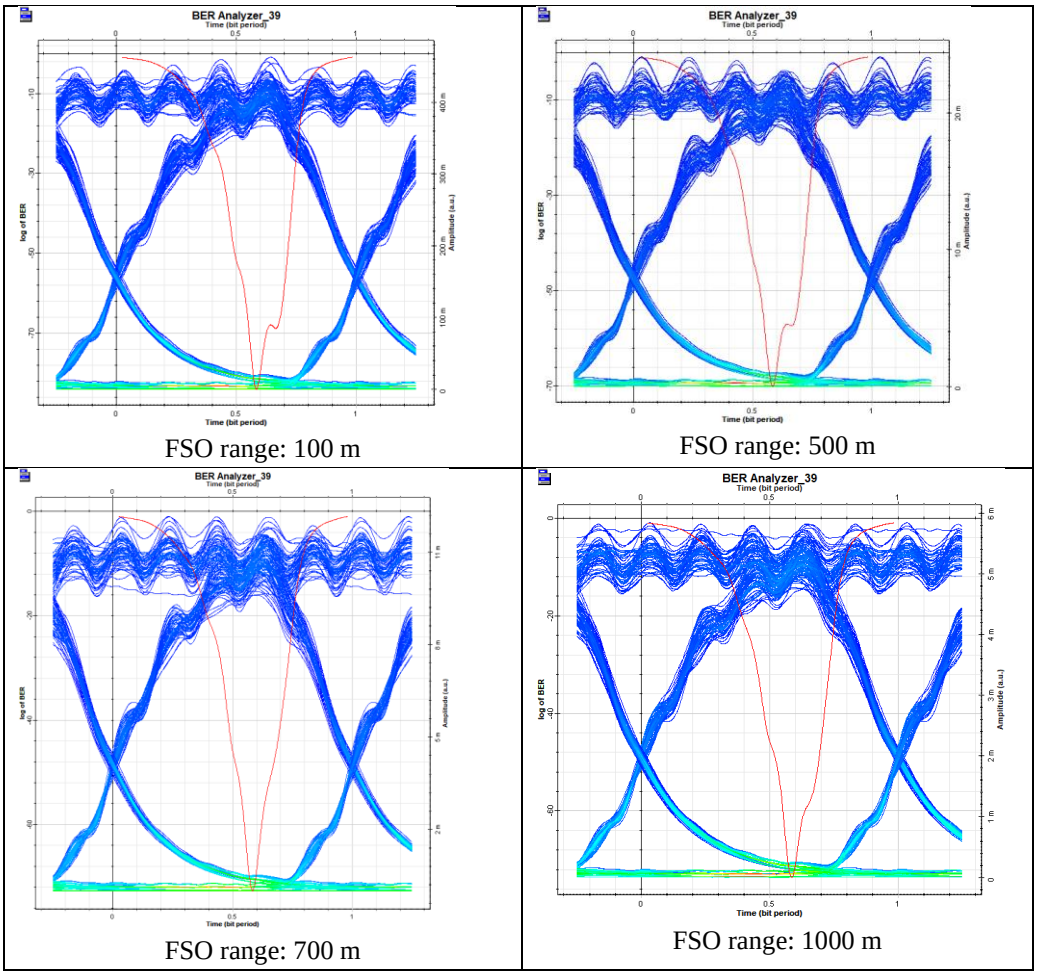


Figure 5.5 Eye diagrams of selected channel for varying FSO range

| **Range of FSO channel (m)** | **BER value** |
|---|---|
| 100 | $1.04 \times 10^{-84}$ |
| 500 | $9.14 \times 10^{-71}$ |
| 700 | $1.85 \times 10^{-73}$ |
| 1000 | $2.4 \times 10^{-74}$ |

Table 5.4 BER values for different range of FSO channel

From the simulation results, we observe from the BER values and eye diagrams that the quality of the received signal is good over a wide range of the FSO transmission channel. Figure 5.6 shows the plot between FSO channel range and BER values for four of the total 89 output channels.

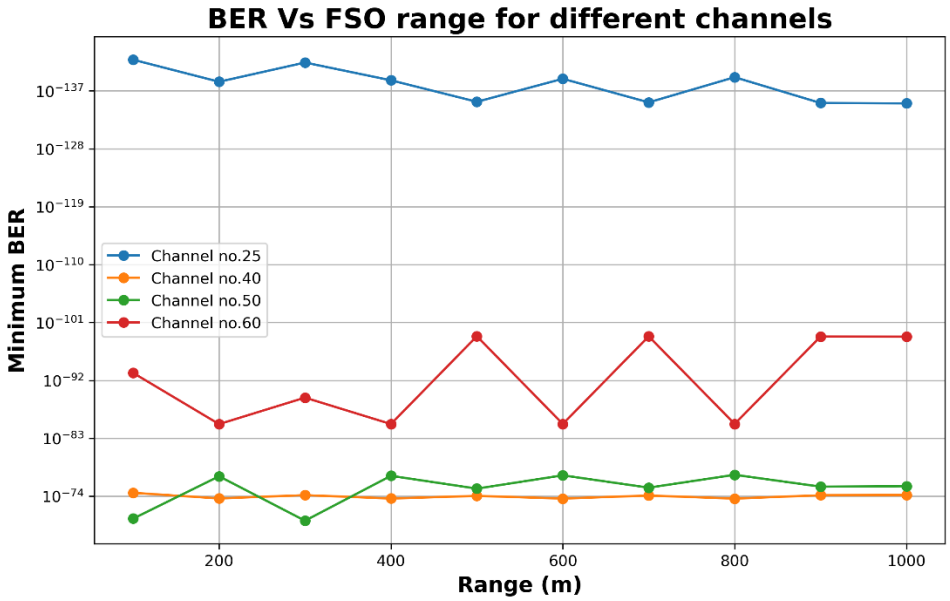


Figure 5.6 Plot between BER and FSO range for four output channels

We can infer from the plot that the quality of the received output signal is good for all the channels considered over a wide transmission range. These results suggest that our proposed system is capable of transmitting high-capacity data over a large transmission range of FSO channel.

It is worthwhile to note that incorporating advanced modelling of FSO channel including scintillation effects can provide more accurate predictions and optimize the system performance. Furthermore, integrating advanced modulation formats such as QPSK (Quadrature Phase Shift Keying), QAM (Quadrature Amplitude Modulation) which offer greater resilience to errors while supporting high data rates can enhance the performance of the system. These techniques not only improve the overall efficiency of the system but also enable more precise predictions further validating and refining our proposed approach.

## 5.5. Summary

In this chapter, conventional DWDM technology is introduced which multiplex several signals and transmitted over a single channel. The transmission medium in DWDM system is usually optical fibre. However, in our work, we have considered free-space medium for transmission of signal. FSO when used in conjunction with DWDM system is cost effective as there is no need of optical fibre infrastructure. One of the main challenges in FSO communication is atmospheric

attenuation and we tried to analyze its effect on different wavelengths of the signal. Attenuation effects for two different wavelengths 750 nm and 1550 nm were found for varying visibility range. It was found that for low visibility range up to 0.5 km the attenuation value remains the same. Hence an important conclusion from this study is that there is no wavelength dependence on attenuation for low visibility range. This refutes the common belief in optical communication that 1550 nm wavelength is less affected by adverse weather conditions. A DWDM system was modelled integrating OFCs for data transmission over FSO channel. OFCs having 89 number of comb lines were demultiplexed and each comb line was modulated with 10 Gbps data. The optical carriers were then multiplexed and transmitted over free space. At the receiver side the signal were demultiplexed and regenerated. Numerical simulations were performed for the modelled system and performance analysis were carried out based on BER and eye diagrams. Based on the simulation results for transmission range of 1 km, the quality of the received signal was good for most of the channels. To further validate the performance of the system the free-space range was varied from 100 m to 1000 m, and we observed that for all the cases the quality of the received signal was robust. In conclusion, this chapter demonstrates the feasibility and effectiveness of integrating OFCs in DWDM systems for high-capacity data transmission over FSO channel, providing a promising approach for next generation communication systems.

# Chapter 6 Conclusion

## 6.1. Summary

In this thesis, we explore the fundamentals of Optical frequency comb and their characteristics. Two methods for OFC generation were studied. In the first method, OFC was generated experimentally using passive mode locked QDash laser. Mode-locking phenomenon of the QDash sample and the characteristics affecting the comb generation were investigated. Experiments were conducted at elevated temperatures, and we observed that with increase in temperature the threshold current increases. We also noticed that with increase in temperature the optical spectrum shifts towards the higher wavelengths. Further experiments analyzed the comb characteristics with increase in bias current. We observed an increase in the bandwidth of the optical spectrum with increase in bias current. Experiments were performed to study the dispersion effects and results showed that with increase in temperature, the dispersion decreased. These studies helped us to better understand the behaviour of mode locked QDash laser sample and offered methods to optimize their performance for practical applications.

In the second method, OFC was generated using fibre loop modulation technique based on electro-optic effect and intracavity active mode locking. Mathematical equations for OFC generation were derived, demonstrating that the comb lines of OFC depend on the modulating RF signal with the frequency spacing between the adjacent combs is equal to the frequency of the modulating signal. Simulations were performed in OptiSystem software to generate OFC using this method and an ultra-broadband OFC was generated having 89 number of comb lines with line spacing of 50 GHz. We also studied the comb characteristics of OFC with respect to the amplitude of the RF signal. Simulation results show that with increase in amplitude of RF signal, the number of comb lines of the OFC increases. Experiments were conducted to generate OFC using this method by our collaborators from Dublin City University. Experimental results were compared with simulation results for the same conditions and a good agreement is obtained between the two.

We have modelled a system to transmit data over free space optical channel using OFC. Studies were conducted on the FSO system to determine the attenuation effect on the wavelength of the signal. Our results show that for a low visibility range of FSO i.e. < 500m, there is no wavelength dependence, and all wavelength signals undergo the same attenuation. For higher visibility range, the longer wavelength signals undergo less attenuation. The proposed system was modelled in

OptiSystem software and simulations were conducted to study the performance of the system. Based on the simulation results, we observe that our proposed system is capable of high-capacity data transmission over FSO channel. This work contributes to the understanding of OFC and its generation methods. Additionally, it also explores the practical application of OFC in DWDM communication system.

## 6.2. Scope for future work

Building upon the findings of this thesis, future work can be focussed on different aspects to improve the performance and efficiency of the system. One promising approach is the use of multiple/cascading modulators in series for generating EO combs which can significantly increase the number of comb lines thereby by broadening the spectral bandwidth. Studies on improved atmospheric models including scintillation effects, different weather conditions like snow, hail etc. will provide more accurate predictions and deeper understanding under various conditions. Advanced data modulation formats like QPSK, QAM can be considered as they offer greater resilience to errors while supporting high-capacity data transmission. Furthermore, OFC based system can be explored for ultra-high-speed transmission pushing the boundaries of data transmission capabilities. Another interesting future approach could be implementing hybrid systems that integrate fibre optics and FSO channel for achieving high-capacity long distance communication. Investigating such systems could provide solutions for bandwidth bottleneck and last mile connectivity. All these collective approaches pave a path for future work for next generation optical communication systems with enhanced efficiency and reliability.

# References


1. Agrell, Erik, et al. “Roadmap on Optical Communications.” Journal of Optics (2010), vol. 26, no. 9, 2024, pp. 93001-, https://doi.org/10.1088/2040-8986/ad261f.

2. Parriaux, Alexandre, et al. “Electro-Optic Frequency Combs.” Advances in Optics and Photonics, vol. 12, no. 1, 2020, pp. 223-, https://doi.org/10.1364/AOP.382052.

3. Dupuis, R. “An Introduction to the Development of the Semiconductor Laser.” IEEE Journal of Quantum Electronics, vol. 23, no. 6, 1987, pp. 651–57, https://doi.org/10.1109/JQE.1987.1073450.

4. Alferov, Zhores I. “Nobel Lecture: The Double Heterostructure Concept and Its Applications in Physics, Electronics, and Technology.” Reviews of Modern Physics, vol. 73, no. 3, 2001, pp. 767–82, https://doi.org/10.1103/RevModPhys.73.767.

5. Bukowski, Tracie J., and Joseph H. Simmons. “Quantum Dot Research: Current State and Future Prospects.” Critical Reviews in Solid State and Materials Sciences, vol. 27, no. 3–4, 2002, pp. 119–42, https://doi.org/10.1080/10408430208500496.

6. Johann Peter Reithmaier, Alfred Forchel, “Recent advances in semiconductor quantum-dot lasers,” Comptes Rendus Physique, Volume 4, Issue 6, 2003, Pages 611-619, ISSN 1631-0705, https://doi.org/10.1016/S1631-0705(03)00075-6

7. Moiseev, Konstantin, et al. “Quantum Dots and Quantum Dashes in the Narrow-Gap InSb/InAsSbP System.” Journal of Crystal Growth, vol. 318, no. 1, 2011, pp. 379–84, https://doi.org/10.1016/j.jcrysgro.2010.10.144.

8. Liu, Guocheng, et al. “Passively Mode-Locked Quantum Dash Laser with an Aggregate 5.376 Tbit/s PAM-4 Transmission Capacity.” Optics Express, vol. 28, no. 4, 2020, pp. 4587–93, https://doi.org/10.1364/OE.386266.

9. Poole, P. J., et al. “Growth of InAs/InP-Based Quantum Dots for 1.55 Mm Laser Applications.” Journal of Crystal Growth, vol. 311, no. 6, 2009, pp. 1482–86, https://doi.org/10.1016/j.jcrysgro.2009.01.129.

10. von der Linde, D. “Characterization of the Noise in Continuously Operating Mode-Locked Lasers.” Applied Physics. B, Lasers and Optics, vol. 39, no. 4, 1986, pp. 201–17, https://doi.org/10.1007/BF00697487.

11. Yadav, Amit, et al. “Edge Emitting Mode-Locked Quantum Dot Lasers.” Progress in Quantum Electronics, vol. 87, 2023, pp. 100451-, https://doi.org/10.1016/j.pquantelec.2022.100451.

12. Piprek, Joachim, editor. Handbook of Optoelectronic Device Modeling and Simulation. Volume Two, Lasers, Modulators, Photodetectors, Solar Cells, and Numerical Methods. CRC Press, 2017.

13. RODWELL, M. J. W., et al. “Reduction of Timing Fluctuations in a Mode-Locked Nd:YAG Laser by Electronic Feedback.” Optics Letters, vol. 11, no. 10, 1986, pp. 638–40, https://doi.org/10.1364/ol.11.000638.

14. Bimberg, Dieter. “Quantum Dots for Lasers, Amplifiers and Computing.” Journal of Physics. D, Applied Physics, vol. 38, no. 13, 2005, pp. 2055–58, https://doi.org/10.1088/0022-3727/38/13/001.

15. Agrawal, G. P. “Effect of Gain Dispersion on Ultrashort Pulse Amplification in Semiconductor Laser Amplifiers.” IEEE Journal of Quantum Electronics, vol. 27, no. 6, 1991, pp. 1843–49, https://doi.org/10.1109/3.90014.

16. Pimenov, A., et al. “Effect of Dynamical Instability on Timing Jitter in Passively Mode-Locked Quantum-Dot Lasers.” Optics Letters, vol. 39, no. 24, 2014, pp. 6815–18, https://doi.org/10.1364/OL.39.006815.

17. Otto, C., et al. “Delay-Induced Dynamics and Jitter Reduction of Passively Mode-Locked Semiconductor Lasers Subject to Optical Feedback.” New Journal of Physics, vol. 14, no. 11, 2012, pp. 113033-, https://doi.org/10.1088/1367-2630/14/11/113033.

18. Arsenijević, D., et al. “Phase Noise and Jitter Reduction by Optical Feedback on Passively Mode-Locked Quantum-Dot Lasers.” Applied Physics Letters, vol. 103, no. 23, 2013, https://doi.org/10.1063/1.4837716

19. TKACH, R. W., and A. R. CHRAPLYVY. “Regimes of Feedback Effects in 1.5-Mm Distributed Feedback Lasers.” Journal of Lightwave Technology, vol. 4, no. 11, 1986, pp. 1655–61, https://doi.org/10.1109/JLT.1986.1074666.

20. Birks, T. A., et al. “Dispersion Compensation Using Single-Material Fibers.” IEEE Photonics Technology Letters, vol. 11, no. 6, 1999, pp. 674–76, https://doi.org/10.1109/68.766781.

21. Faugeron, M., et al. “High Peak Power, Narrow RF Linewidth Asymmetrical Cladding Quantum-Dash Mode-Locked Lasers.” IEEE Journal of Selected Topics in Quantum Electronics, vol. 19, no. 4, 2013, pp. 1101008–1101008, https://doi.org/10.1109/JSTQE.2013.2241025.

22. Schaefer, Sebastian, “Numerical Simulation and Experimental Investigation of Quantum Dash Lasers at Elevated Temperatures: Design and Operation of Monolithic InAs/InP Quantum Dash Ridge Laser Diodes Operating in the C-Band”, PhD thesis, 2024. Université d’Ottawa / University of Ottawa.

23. Leesti, Bertram. Cross-Gain Modulation and Four-Wave Mixing with Picosecond Pulses in a Quantum-Dash Waveguide. 2004. University of Toronto, ProQuest Dissertations & Theses.

24. Lu, Zhenguo, et al. “Quantum Dash Multi-Wavelength Lasers for Tbit/s Coherent Communications and 5G Wireless Networks.” Journal of the European Optical Society. Rapid Publications, vol. 17, no. 1, 2021, pp. 1–7, https://doi.org/10.1186/s41476-021-00156-9.

25. Lu, Z. G., et al. “A Passive Mode-Locked InAs/InP Quantum Dot Laser with Pulse Duration of Less than 300 Fs.” Proceedings of SPIE, vol. 7224, no. 1, SPIE, 2009, pp. 722413–17, https://doi.org/10.1117/12.809525.

26. Hirano, Masaki, and Akihiro Morimoto. “Generation of Flat Optical Frequency Comb by Fiber Loop Modulation.” Optical Review (Tokyo, Japan), vol. 18, no. 1, 2011, pp. 13–18, https://doi.org/10.1007/s10043-011-0009-z.

27. Chang, Lin, et al. “Integrated Optical Frequency Comb Technologies.” Nature Photonics, vol. 16, no. 2, 2022, pp. 95–108, https://doi.org/10.1038/s41566-021-00945-1.

28. SAKAMOTO, Takahide, et al. “Asymptotic Formalism for Ultraflat Optical Frequency Comb Generation Using a Mach-Zehnder Modulator.” Optics Letters, vol. 32, no. 11, 2007, pp. 1515–17, https://doi.org/10.1364/ol.32.001515.

29. Zhuang, Rongjin, et al. “Electro-Optic Frequency Combs: Theory, Characteristics, and Applications.” *Laser & Photonics Reviews*, vol. 17, no. 6, 2023, https://doi.org/10.1002/lpor.202200353.

30. Luntadila Lufungula, Isaac, et al. “Integrated Resonant Electro-Optic Comb Enabled by Platform-Agnostic Laser Integration.” Laser & Photonics Reviews, vol. 18, no. 10, 2024, https://doi.org/10.1002/lpor.202400205.

31. Lundberg, Lars, et al. “Frequency Comb-Based WDM Transmission Systems Enabling Joint Signal Processing.” Applied Sciences, vol. 8, no. 5, 2018, pp. 718-, https://doi.org/10.3390/app8050718.

32. Kim, Isaac I., et al. “Comparison of Laser Beam Propagation at 785 Nm and 1550 Nm in Fog and Haze for Optical Wireless Communications.” Proceedings of SPIE, vol. 4214, no. 1, SPIE, 2001, pp. 26–37, https://doi.org/10.1117/12.417512.

33. Szajowski, Paul F., et al. “Key Elements of High-Speed WDM Terrestrial Free-Space Optical Communications Systems.” Proceedings of SPIE, vol. 3932, no. 1, SPIE, 2000, pp. 2–14, https://doi.org/10.1117/12.384300.

34. Trichili, Abderrahmen, et al. “Roadmap to Free Space Optics.” Journal of the Optical Society of America. B, Optical Physics, vol. 37, no. 11, 2020, pp. A184-, https://doi.org/10.1364/JOSAB.399168.

35. Al-Gailani, Samir Ahmed, et al. “A Survey of Free Space Optics (FSO) Communication Systems, Links, and Networks.” IEEE Access, vol. 9, 2021, pp. 7353–73, https://doi.org/10.1109/ACCESS.2020.3048049.

36. Jahid, Abu, et al. “A Contemporary Survey on Free Space Optical Communication: Potentials, Technical Challenges, Recent Advances and Research Direction.” Journal of Network and Computer Applications, vol. 200, 2022, pp. 103311-, https://doi.org/10.1016/j.jnca.2021.103311.

37. Li, Chung-Yi, et al. “A WDM PAM4 FSO-UWOC Integrated System With a Channel Capacity of 100 Gb/s.” Journal of Lightwave Technology, vol. 38, no. 7, 2020, pp. 1766–76, https://doi.org/10.1109/JLT.2019.2960525.

38. Jiang, Pan, et al. “Broadband Optical Frequency Comb Generation Based on Single Electro-Absorption Modulation Driven by Radio Frequency Coupled Signals.” Frontiers of Optoelectronics (Online), vol. 15, no. 4, 2022, pp. 45–45, https://doi.org/10.1007/s12200-022-00045-0.

39. Hao Zhang, et al. “Coherent Optical Frequency Combs: From Principles to Applications.” Journal of Electronic Science and Technology, vol. 20, no. 2, 2022, pp. 100157-.

40. Torres-Company, Victor, et al. “Laser Frequency Combs for Coherent Optical Communications.” Journal of Lightwave Technology, vol. 37, no. 7, 2019, pp. 1663–70, https://doi.org/10.1109/JLT.2019.2894170.

41. Ho, K. P., and J. M. Kahn. “Optical Frequency Comb Generator Using Phase Modulation in Amplified Circulating Loop.” IEEE Photonics Technology Letters, vol. 5, no. 6, 1993, pp. 721–25, https://doi.org/10.1109/68.219723.

42. Tan, Zeyu, and Lirong Huang. “Optical-Frequency-Comb Generation Based on Single-Tone Modulation and Four-Wave Mixing Effect in One Single Semiconductor Optical Amplifier.” Photonics, vol. 9, no. 10, 2022, pp. 746-, https://doi.org/10.3390/photonics9100746.